ANTIOXIDANTS & REDOX SIGNALING
Volume 28, Number 6, 2018
Mary Ann Liebert, Inc.
DOI: 10.1089/ars.2016.6897

FORUM ORIGINAL RESEARCH COMMUNICATION

# Protein *S*-Bacillithiolation Functions in Thiol Protection and Redox Regulation of the Glyceraldehyde-3-Phosphate Dehydrogenase Gap in *Staphylococcus aureus* Under Hypochlorite Stress

Marcel Imber,[1,*] Nguyen Thi Thu Huyen,[1,*] Agnieszka J. Pietrzyk-Brzezinska,[2,*] Vu Van Loi,[1,*] Melanie Hillion,[1] Jörg Bernhardt,[3] Lena Thärichen,[4,5] Katra Kolšek,[5] Malek Saleh,[1] Chris J. Hamilton,[6] Lorenz Adrian,[7] Frauke Gräter,[4,5] Markus C. Wahl,[2] and Haike Antelmann[1]

**Abstract**

***Aims:*** Bacillithiol (BSH) is the major low-molecular-weight thiol of the human pathogen *Staphylococcus aureus*. In this study, we used OxICAT and *Voronoi redox treemaps* to quantify hypochlorite-sensitive protein thiols in *S. aureus* USA300 and analyzed the role of BSH in protein *S*-bacillithiolation.

***Results:*** The OxICAT analyses enabled the quantification of 228 Cys residues in the redox proteome of *S. aureus* USA300. Hypochlorite stress resulted in >10% increased oxidation of 58 Cys residues (25.4%) in the thiol redox proteome. Among the highly oxidized sodium hypochlorite (NaOCl)-sensitive proteins are five *S*-bacillithiolated proteins (Gap, AldA, GuaB, RpmJ, and PpaC). The glyceraldehyde-3-phosphate (G3P) dehydrogenase Gap represents the most abundant *S*-bacillithiolated protein contributing 4% to the total Cys proteome. The active site Cys151 of Gap was very sensitive to overoxidation and irreversible inactivation by hydrogen peroxide ($H_2O_2$) or NaOCl *in vitro*. Treatment with $H_2O_2$ or NaOCl in the presence of BSH resulted in reversible Gap inactivation due to *S*-bacillithiolation, which could be regenerated by the bacilliredoxin Brx (SAUSA300_1321) *in vitro*. Molecular docking was used to model the *S*-bacillithiolated Gap active site, suggesting that formation of the BSH mixed disulfide does not require major structural changes.

***Conclusion and Innovation:*** Using OxICAT analyses, we identified 58 novel NaOCl-sensitive proteins in the pathogen *S. aureus* that could play protective roles against the host immune defense and include the glycolytic Gap as major target for *S*-bacillithiolation. *S*-bacillithiolation of Gap did not require structural changes, but efficiently functions in redox regulation and protection of the active site against irreversible overoxidation in *S. aureus*. *Antioxid. Redox Signal*. 28, 410–430.

**Keywords:** *Staphylococcus aureus*, *S*-bacillithiolation, thiol-redox proteomics, Gap, bacilliredoxin

[1]Institute for Biology-Microbiology and [2]Laboratory of Structural Biochemistry, Freie Universität Berlin, Berlin, Germany.
[3]Institute for Microbiology, Ernst-Moritz-Arndt-Universität of Greifswald, Greifswald, Germany.
[4]Molecular Biomechanics, Interdisciplinary Center for Scientific Computing (IWR), Heidelberg University, Heidelberg, Germany.
[5]Heidelberg Institute of Theoretical Studies, Heidelberg, Germany.
[6]School of Pharmacy, University of East Anglia, Norwich Research Park, Norwich, United Kingdom.
[7]Department Isotope Biogeochemistry, Helmholtz Centre for Environmental Research-UFZ, Leipzig, Germany.
*These authors contributed equally to this work.

### Innovation

Using quantitative redox proteomics, 58 redox-sensitive protein thiols were identified in the methicillin-resistant *Staphylococcus aureus* strain USA300 that showed >10% increased oxidation under NaOCl stress. The glyceraldehyde-3-phosphate dehydrogenase Gap was identified as most abundant target for thiol oxidation and represents the major *S*-bacillithiolated protein in *S. aureus* cells. Molecular docking of bacillithiol (BSH) into the active site suggests that *S*-bacillithiolation does not require major structural changes. Finally, our biochemical assays confirm that *S*-bacillithiolation efficiently protects the Gap active site against overoxidation by $H_2O_2$ and NaOCl and inhibits Gap activity, which can be reversed by the bacilliredoxin Brx *in vitro*.

## Introduction

*STAPHYLOCOCCUS AUREUS* is a common commensal bacterium that colonizes the anterior nares and the skin of one quarter of the human population without causing symptoms of infections (22). However, *S. aureus* can also cause infections ranging from local skin or soft tissue infections to life-threatening diseases, such as septicemia, endocarditis, and necrotizing pneumonia, when the pathogen enters the bloodstream (2, 8, 53). Many nosocomial infections are caused by multiple antibiotic-resistant strains, such as methicillin-resistant *S. aureus* (MRSA) isolates (50). Moreover, new community-acquired MRSA strains are emerging quickly with other strains that are resistant to the last resort of antibiotics, such as vancomycin (22). Thus, to understand the adaptation of the pathogen to the host defense, it is of utmost importance to identify new drug targets for the treatment of MRSA infections.

The success of *S. aureus* as a leading pathogen is caused by high diversity of different virulence factors, such as toxins, proteases, lipases, and superantigens, as well as efficient protection mechanisms against the host immune defense during invasion. During infections, *S. aureus* has to cope with the oxidative burst of activated macrophages and neutrophils, including reactive oxygen and nitrogen species (ROS, RNS) and the strong oxidant hypochlorous acid (HOCl) (75, 76). HOCl is produced in neutrophils by the enzyme myeloperoxidase (MPO) from hydrogen peroxide ($H_2O_2$) and chloride (44). The involvement of HOCl as prime mechanism for oxidative killing of *S. aureus* by neutrophils has been shown using MPO inhibitors (29). Moreover, killing of many bacteria by isolated neutrophils is strongly inhibited in the absence of MPO (44).

*S. aureus* uses several redox-sensing virulence regulators, such as SarA and the MarR/OhrR-type regulators, MgrA and SarZ, for defense against oxidative stress. These control large regulons of virulence factors, antibiotic resistance determinants, and ROS detoxification enzymes (11–13, 35). MgrA and SarZ are both single Cys MarR/OhrR-type repressors that sense and respond to ROS *via* thiol-based redox switches and by Cys phosphorylation (63, 70). In addition, *S. aureus* uses the low-molecular-weight (LMW) thiol bacillithiol (BSH, Cys-GlcNAc-Mal) to maintain the reduced state of the cytoplasm. BSH plays an important role in detoxification of redox-active compounds in *S. aureus* since *bshA* mutants displayed increased sensitivities to ROS, hypochlorite, electrophiles, and the antibiotic fosfomycin (52, 64, 65). Moreover, BSH mediates protection under infection-like conditions as shown in phagocytosis assays using human macrophages (64, 65). Apart from BSH, also CoenzymeA (CoASH) and cysteine are found as abundant alternative LMW thiols in *S. aureus* cells (58).

Under hypochlorite stress, we have shown that BSH is also used for *S*-thiolation of redox-sensitive Cys residues and forms mixed disulfides with proteins that are termed as *S*-bacillithiolation. *S*-bacillithiolation protects protein thiols against overoxidation to sulfonic acids and is an important redox regulatory device in Firmicutes analogous to *S*-glutathionylation in eukaryotes (15, 16, 47, 52). The presence of CoASH and cysteine as LMW thiols suggests that alternative *S*-thiolations are also possible in *S. aureus*, such as *S*-cysteinylation or CoASH mixed disulfides. In support of this notion, *S. aureus* encodes a CoASH disulfide reductase (Cdr) that functions in reduction of CoASH mixed protein disulfides (55).

Using shotgun proteomics, we have previously identified 54 *S*-bacillithiolated proteins in different *Bacillus species* and *Staphylococcus carnosus* (16). Among these are eight conserved *S*-bacillithiolated proteins, such as the methionine synthase MetE, the inorganic pyrophosphatase PpaC, and the inosine-5′-monophosphate (IMP) dehydrogenase GuaB. The glutaredoxin-like YphP protein of the UPF0403 family was also *S*-bacillithiolated in *Bacillus subtilis in vivo* at its CGC active site motif (15). YphP and its paralog YqiW were renamed as BrxA and BrxB based on their function as bacilliredoxins in the reduction of *S*-bacillithiolated OhrR and MetE *in vitro* (24). Reduction of *S*-bacillithiolated proteins leads to Brx-SSB formation, which requires BSH and a still unknown BSSB reductase for recycling (24, 25, 31, 52). We have recently fused the YphP homolog (Brx) of *S. aureus* USA300 (SAUSA300_1321) to roGFP2 to construct a dynamic biosensor to monitor BSH redox potential changes *in vivo* (51). Brx-roGFP2 was highly specific to recognize BSSB, which confirms the role of Brx as bacilliredoxin also in *S. aureus*.

The physiological role of *S*-bacillithiolation in redox regulation has been demonstrated for the redox-sensing OhrR repressor and the methionine synthase MetE under hypochlorite stress in *B. subtilis*. *S*-bacillithiolation of MetE in its active site Zn center leads to its inactivation and subsequent methionine auxotrophy (15). The DNA-binding activity of the organic hydroperoxide repressor, OhrR, is inhibited by *S*-bacillithiolation under sodium hypochlorite (NaOCl) and cumene hydroperoxide stress, which results in the expression of the OhrA peroxiredoxin as ROS protection mechanism (15, 47).

However, the targets for *S*-bacillithiolation or reversible thiol oxidation under hypochlorite stress are unknown in the major pathogen *S. aureus*, which could provide leads in drug design to treat MRSA infections. In this study, we have combined the quantitative redox proteomic approach OxICAT (9, 48, 49) and shotgun proteomics to quantify NaOCl-sensitive proteins and to identify *S*-bacillithiolated proteins in *S. aureus* USA300. We found that 25% protein thiols showed >10% increased oxidation under NaOCl stress. The glycolytic Gap was identified as the most abundant *S*-bacillithiolated protein in *S. aureus*. Our results document that *S*-bacillithiolation protects the active site against overoxidation and inhibits Gap activity *in vitro*.

## Results

### *Identification of 58 NaOCl-sensitive proteins using the quantitative redox proteomic approach OxICAT in* S. aureus *USA300*

We were interested to study the role of BSH for *S*-bacillithiolation and the global thiol oxidation state under hypochlorite stress in the major pathogen *S. aureus*. Thus, we performed a quantitative thiol redox proteomic approach based on OxICAT (48, 49) and analyzed the percentages of thiol oxidation levels in *S. aureus* USA300 in response to 150 $\mu M$ NaOCl stress, as determined previously (51). OxICAT is based on the differential thiol labeling of reduced Cys residues with light isotope-coded affinity tag ($^{12}$C-ICAT), followed by reduction of reversible thiol oxidation (*e.g.,* protein disulfides and *S*-thiolation) with Tris (2-carboxyethyl) phosphine (TCEP) and subsequent labeling of previously oxidized thiols with heavy $^{13}$C-ICAT reagent (48). Light and heavy ICAT-labeled peptide pairs show a mass difference of 9 Da after separation using mass spectrometry (MS). The quantification of the percentage of thiol oxidation for each Cys peptide is based on the calculation of the intensity of the heavy ICAT-labeled Cys peptide in relation to the total intensity of the light and heavy ICAT-labeled Cys peptides.

The OxICAT analysis enabled the quantification of the percentages of reversible thiol oxidation for 228 Cys peptides in the thiol redox proteome of *S. aureus* USA300 (Supplementary Table S1; Supplementary Data; Supplementary Data are available online at www.liebertpub.com/ars). The percentages of thiol oxidation were color coded and visualized in *Voronoi redox treemaps* according to the TIGRfam classification of *S. aureus* USA300 (Fig. 1).

In untreated *S. aureus* cells, we identified 193 Cys residues (84.6%) with a thiol oxidation level of <25%, including 107 Cys residues (46.9%) with <10% oxidation, indicating that the majority of thiols are in a reduced state (Tables 1 and 2; Supplementary Table S1). Only 35 Cys residues (15.3%) showed basal-level oxidation of >25% in the control. These

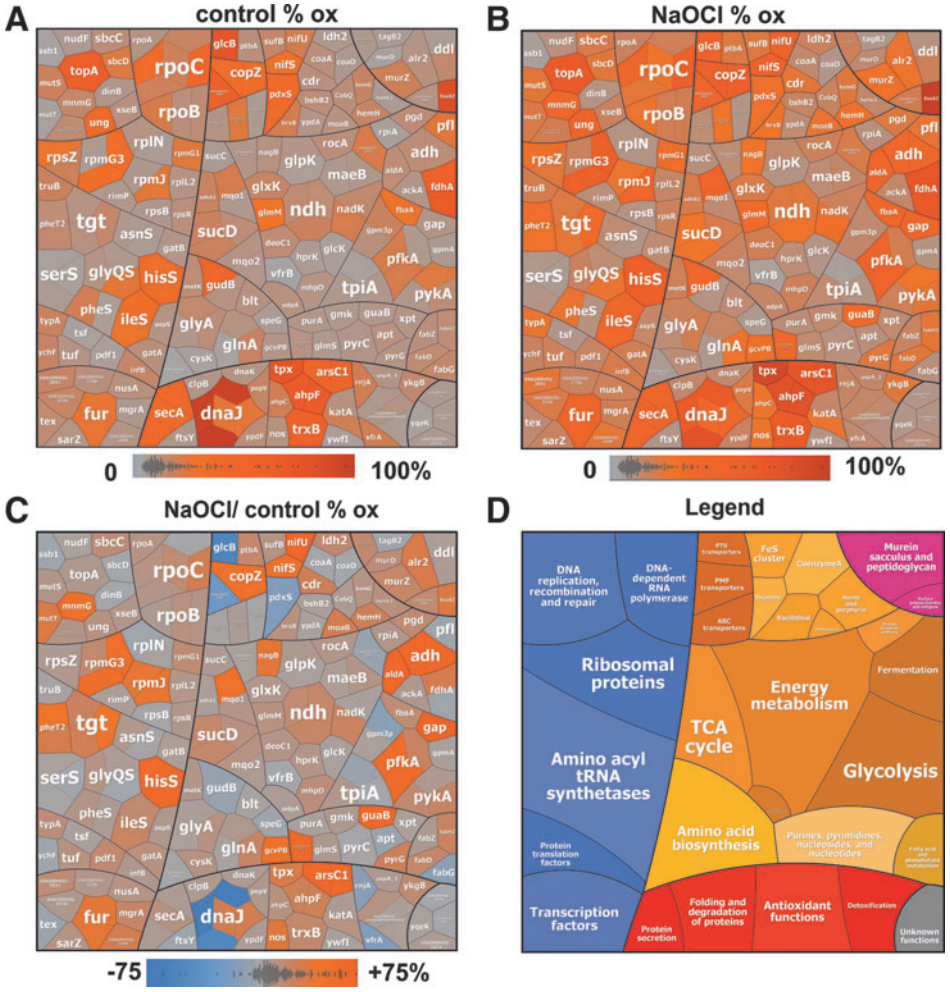


**FIG. 1. Percentages of thiol oxidation for 228 Cys peptides that are identified in *Staphylococcus aureus* USA300 and visualized using *Voronoi redox treemaps*.** The percentages of thiol oxidation of 228 Cys residues that are identified using OxICAT in *S. aureus* USA300 in the control **(A)** and 30 min after exposure to 150 $\mu M$ NaOCl stress **(B)** are visualized using *Voronoi redox treemaps*. The *gray–red* color gradient denotes 0–100% oxidation. The *Voronoi redox treemap* in **(C)** shows the percentages of oxidation changes under NaOCl stress using a *blue–red* color gradient ranging from −75% to +75% oxidation. The treemap in **(D)** serves as the legend showing the functional classifications of proteins. The treemaps are generated using the Paver software (Decodon) based on the OxICAT data presented in Supplementary Tables S1 and proteins were classified according to the *S. aureus* USA300 TIGRfam annotation. NaOCl, sodium hypochlorite.

Table 1. Overview of % Thiol Oxidation of 228 Cys Residues in the Redox Proteome of *Staphylococcus aureus*

| 228 Cys residues | **<25% (<10%)** | **>25% (>40%)** |
|---|---|---|
| % Thiol oxidation Control | **193 (107)** 84.6% (46.9%) | **35 (15)** 15.3% (6.6%) |
| % Thiol oxidation NaOCl | **159 (35)** 69.7% (15.3%) | **69 (27)** 30.2% (11.8%) |
| | **<10%** | **>10% (20–30%)** |
| % Thiol oxidation increase (NaOCl/Control) | **170** 74.6% | **58 (19)** 25.4% (8.3%) |

Overview of % thiol oxidation of 228 Cys peptides identified in the redox proteome of the *S. aureus* USA300 under control and NaOCl stress, as revealed by OxICAT. All reduced Cys peptides have an oxidation degree of <25% that include those with <10% oxidation, shown in parenthesis. Oxidized Cys peptides have an oxidation degree of >25%. The % thiol oxidation increase includes Cys peptides with no significant increased oxidation (<10%) and those with >10% increased oxidation in response to NaOCl stress compared with the control. The % thiol-oxidation and % thiol-oxidation increase and related Cys numbers are shown in *bold-faced*. The percentage of Cys numbers in relation to all Cys residues is shown in *non-bold faced*.

NaOCl, sodium hypochlorite.

basal-level oxidized proteins include predicted redox-sensitive proteins (21), such as the thiol peroxidase Tpx, the alkyl hydroperoxide reductase large subunit AhpF, the arsenate reductase ArsC1, and the thioredoxin reductase TrxB1. Tpx and AhpCF were previously found as basal-level oxidized in the redox proteomes of *Escherichia coli* and *Bacillus* species (16, 48). Tpx was also S-mycothiolated in *Corynebacterium glutamicum* at the conserved active site Cys60 (14). In addition, the topoisomerase TopA and the DnaJ chaperone are basal-level oxidized at their Zn-binding Cys residues.

To discover novel NaOCl-sensitive proteins, we analyzed the percentages of thiol oxidation levels under NaOCl stress and its oxidation increase using OxICAT (Fig. 1 and Tables 2; Supplementary Table S1). The OxICAT approach enabled the identification of 58 NaOCl-sensitive Cys residues (25.4%) with >10% increased oxidation, including 19 Cys residues with 20–30% oxidation change under NaOCl stress (Tables 1 and 2 and Supplementary Table S1). Several NaOCl-sensitive proteins have antioxidant functions, such as the AhpCF peroxiredoxins, the thioredoxin reductase TrxB1, and the arsenate reductase ArsC. Furthermore, interesting proteins are the nitric oxide synthase (USA300HOU_1916) and the CoASH disulfide reductase Cdr (USA300HOU_0929), the latter is oxidized at the conserved Cys16. Apart from Cdr, the putative BSH disulfide reductase YpdA (USA300GOU_1417) was oxidized at the same conserved Cys14, but its oxidation is not increased under NaOCl stress (Supplementary Table S1). Moreover, we observed a slightly increased oxidation of the deacetylase BshB2 involved BSH biosynthesis and of the bacilliredoxin YqiW (BrxB) under NaOCl stress. The oxidation of Cdr, YpdA, BshB2, and BrxB could indicate increased *S*-bacillithiolation and CoASH mixed protein disulfides under NaOCl stress.

NaOCl-sensitive proteins are often oxidized in CxxC motifs and at conserved Zn-binding sites. Examples for Zn redox switches are the Zn-containing alcohol dehydrogenase Adh (USA300HOU_0610), the ribosomal proteins RpmG3 (USA300HOU_1553), and RpmJ (USA300HOU_2218). Zn-containing ribosomal proteins share three to four Cys residues that are suggested to serve as reservoir for Zn storage (54). As another Zn redox switch, we identified the ferric uptake repressor Fur that showed 16.6% increased oxidation at its Zn-binding site at Cys 140 and Cys143 under NaOCl stress (Tables 2; Supplementary Table S1; Figs. 1–2). Fur contains two CxxC motifs that form a structural Cys4:Zn site and are required for stability. In addition, two regulatory iron-binding sites are present in Fur (32). FurA of *Anabaena* was described as redox switch under oxidative stress and Cys101 in the CxxC motif is essential for iron-sensing and DNA-binding activity (7).

The copper chaperone CopZ was 19.8% oxidized in its CxxC motif that is required for Cu binding (67). The interaction of the *B. subtilis* CopZ homolog with BSH has been recently studied leading to the formation of *S*-bacillithiolated apo-CopZ and Cu(i)-bound forms of CopZ (42). In addition, NaOCl-sensitive Cys residues often coordinate FeS clusters or function in FeS cluster biogenesis. The FeS cluster scaffold protein NifU showed 26% increased oxidation at Cys41 that binds the FeS cluster during the assembly. The cysteine desulfurase NifS exhibits 20.6% higher oxidation levels at the catalytic Cys371 that forms the persulfide with the sulfur released during cysteine desulfuration (5). In addition, the FeS cluster assembly protein SufB is oxidized in its FeS cluster binding Cys302. It is interesting to note that the *nifS-nifU-sufB* genes are cotranscribed in an operon.

As NaOCl-sensing redox regulators, the MarR/OhrR family repressors, MgrA and SarZ (USA300HOU_0709 and USA300HOU_2368), were identified that showed 10.5% and 6.5% increased oxidation levels under NaOCl stress at their redox-sensing single Cys (Fig. 2). The DNA-binding activity of MgrA and SarZ was inhibited by *S*-thiolation using a synthetic thiol *in vitro* (11, 13, 35). In this study, increased oxidation of MgrA and SarZ was found in *S. aureus* under NaOCl stress, indicating that both could be redox controlled by *S*-bacillithiolation analogous to OhrR of *B. subtilis* (47). OhrR and SarZ both control a homologous *ohrA* peroxiredoxin gene that confers resistance to organic hydroperoxides and NaOCl in *B. subtilis* (13). Northern blot analyses revealed increased transcription of *ohrA* under NaOCl stress, indicating that SarZ oxidation leads to its inactivation and derepression of *ohrA* transcription (Fig. 3). We further noted the 15% increased oxidation of the virulence factor and secretory antigen SsaA2 at its conserved single Cys171 under NaOCl stress. The homologous SceB precursor (Sca_1790) of *S. carnosus* was previously *S*-bacillithiolated at the conserved Cys in NaOCl-treated cells (16). Thus, SsaA2 is most likely also *S*-bacillithiolated in *S. aureus*.

The NaOCl-sensitive proteins of *S. aureus* include many metabolic enzymes that function in energy metabolism and in different biosynthesis pathways for amino acids, fatty acids, nucleotides, and cofactors. NaOCl-sensitive enzymes involved in energy metabolism include the glycolytic glyceraldehyde-3-phosphate (G3P) dehydrogenase Gap and phosphofructokinase PfkA (USA300HOU_1685), the alcohol dehydrogenase Adh, the aldehyde dehydrogenase AldA (USA300HOU_2110), the formate dehydrogenase FdhA (USA300HOU_2291), and the malate dehydrogenase Mqo (USA300HOU_2348). Gap and AldA both showed the highest oxidation increase of 29% and 26% under NaOCl stress at their

TABLE 2. QUANTIFICATION OF 58 CYS PEPTIDES WITH REVERSIBLE THIOL OXIDATION THAT SHOWED >10% INCREASED OXIDATION IN *STAPHYLOCOCCUS AUREUS* USA300 UNDER NAOCL STRESS USING THE OXICAT APPROACH

| *Locus tag* | *Gene name* | *Protein function* | *Cys* | *Buried/ Exposed* | *RSA (%)* | *% Diff NaOCl/Co* | *Mean % oxidation control* | *CV* | *Mean % oxidation NaOCl* | *CV* |
|---|---|---|---|---|---|---|---|---|---|---|
| **Cell envelope function** | | | | | | | | | | |
| USA300HOU_2065 | alr2 | Alanine racemase | Cys311[a] | B | 3.7 | **14.56** | 8.22 | 0.16 | 22.79 | 0.14 |
| USA300HOU_2065 | alr2 | Alanine racemase | Cys304 | B | 8.7 | **13.89** | 9.86 | 0.11 | 23.75 | 0.08 |
| USA300HOU_2112 | murZ | UDP-N-acetylglucosamine 1-carboxyvinyltransferase | Cys110 | B | 7.7 | **10.03** | 16.57 | 0.10 | 26.60 | 0.16 |
| USA300HOU_2112 | murZ | UDP-N-acetylglucosamine 1-carboxyvinyltransferase | Cys118[a] | E | 56.2 | **10.03** | 16.57 | 0.10 | 26.60 | 0.16 |
| USA300HOU_2280 | SsaA2 | Secretory antigen SsaA2 | Cys171[a] | B | 1.3 | **14.94** | 71.35 | 0.14 | 86.29 | 0.02 |
| **Protein quality control (Chaperones and proteases)** | | | | | | | | | | |
| USA300HOU_1580 | dnaJ | Chaperone DnaJ | Cys149[a] | B | 8.3 | **13.44** | 21.81 | 0.43 | 35.24 | 0.10 |
| USA300HOU_1580 | dnaJ | Chaperone DnaJ | Cys152[a] | B | 24.7 | **13.44** | 21.81 | 0.43 | 35.24 | 0.10 |
| **Detoxification and adaptation to atypical environments** | | | | | | | | | | |
| USA300HOU_1700 | tpx[#] | Thiol peroxidase | Cys60[a] | B | 2.6 | **14.48** | 62.73 | 0.05 | 77.21 | 0.02 |
| USA300HOU_0403 | ahpF[#] | Peroxiredoxin subunit F | Cys335[a] | B | 3.3 | **12.54** | 56.65 | 0.08 | 69.19 | 0.05 |
| USA300HOU_0403 | ahpF[#] | Peroxiredoxin subunit F | Cys338[a] | B | 7.5 | **12.54** | 56.65 | 0.08 | 69.19 | 0.05 |
| USA300HOU_0839 | arsC1[#] | Arsenate reductase | Cys10[a] | B | 10.1 | **24.59** | 38.55 | 0.11 | 63.14 | 0.12 |
| USA300HOU_0839 | arsC1[#] | Arsenate reductase | Cys13[a] | B | 8.9 | **24.59** | 38.55 | 0.11 | 63.14 | 0.12 |
| USA300HOU_1916 | nos | Nitric oxide synthase | Cys131 | B | 10.9 | **15.52** | 9.34 | 0.03 | 24.85 | 0.53 |
| **DNA replication, recombination, and repair** | | | | | | | | | | |
| USA300HOU_2714 | mnmG | Glucose-inhibited division protein A | Cys274[a] | B | 13.4 | **20.86** | 13.36 | 0.41 | 34.22 | 0.18 |
| USA300HOU_2481 | mutT | Mutator protein mutT | Cys87 | B | 1.5 | **14.82** | 4.45 | 0.25 | 19.26 | 0.19 |
| **Transcription and transcriptional regulators** | | | | | | | | | | |
| USA300HOU_1499 | fur | Fur repressor | Cys140[a] | B | 3.1 | **16.63** | 22.73 | 0.51 | 39.36 | 0.30 |
| USA300HOU_1499 | fur | Fur repressor | Cys143[a] | B | 7.5 | **16.63** | 22.73 | 0.51 | 39.36 | 0.30 |
| USA300HOU_0709 | mgrA | MarR/OhrR transcriptional regulator MgrA | Cys12 | B | 5.0 | **10.46** | 6.62 | 0.11 | 17.08 | 0.02 |
| USA300HOU_2368 | sarZ | MarR/OhrR transcriptional regulator SarZ | Cys13 | B | 4.2 | **6.31** | 8.43 | 0.29 | 14.73 | 0.07 |
| USA300HOU_1199 | USA300HOU_1199 | Nucleic acid-binding, transcription termination | Cys11[a] | B | 2.8 | **13.33** | 8.21 | 0.35 | 21.54 | 0.38 |
| USA300HOU_0537 | rpoC | RNA polymerase subunit beta' | Cys75[a] | B | 4.3 | **13.00** | 37.68 | 0.11 | 50.69 | 0.08 |

(*continued*)

TABLE 2. (CONTINUED)

| *Locus tag* | *Gene name* | *Protein function* | *Cys* | *Buried/ Exposed* | *RSA (%)* | *% Diff NaOCl/Co* | *Mean % oxidation control* | *CV* | *Mean % oxidation NaOCl* | *CV* |
|---|---|---|---|---|---|---|---|---|---|---|
| **Translation (Aminacyl tRNA synthetases, translation factors, and ribosomal proteins)** | | | | | | | | | | |
| Amino acyl tRNA synthetases | | | | | | | | | | |
| USA300HOU_1629 | hisS | Histidine-tRNA ligase | Cys191 | B | 8.5 | **24.59** | 29.40 | 0.25 | 53.99 | 0.10 |
| USA300HOU_1629 | hisS | Histidine-tRNA ligase | Cys194 | B | 4.3 | **24.59** | 29.40 | 0.25 | 53.99 | 0.10 |
| USA300HOU_1130 | ileS | Isoleucine-tRNA ligase | Cys124[a] | B | 0.9 | **10.77** | 23.74 | 0.18 | 34.51 | 0.03 |
| USA300HOU_1732 | pheT2 | Phenylalanine-tRNA ligase beta subunit | Cys126[a] | B | 4.0 | **18.48** | 11.13 | 0.74 | 29.61 | 0.01 |
| USA300HOU_1732 | pheT2 | Phenylalanine-tRNA ligase beta subunit | Cys167[a] | B | 2.0 | **13.79** | 12.38 | 0.29 | 26.17 | 0.05 |
| USA300HOU_1638 | tgt | Queuine tRNA-ribosyltransferase | Cys12[a] | B | 15.2 | **12.73** | 9.32 | 0.07 | 22.04 | 0.42 |
| USA300HOU_1638 | tgt | Queuine tRNA-ribosyltransferase | Cys281[a] | B | 2.5 | **18.74** | 13.36 | 0.25 | 32.10 | 0.14 |
| USA300HOU_1638 | tgt | Queuine tRNA-ribosyltransferase | Cys174[a] | B | 1.5 | **11.40** | 8.79 | 0.00 | 20.19 | 0.34 |
| Ribosomal proteins: synthesis and modification | | | | | | | | | | |
| USA300HOU_1553 | rpmG3 | Ribosomal protein L33 | Cys9[a] | B | 3.9 | **21.76** | 29.30 | 0.02 | 51.06 | 0.04 |
| USA300HOU_1553 | rpmG3 | Ribosomal protein L33 | Cys12[a] | B | 25.6 | **21.76** | 29.30 | 0.02 | 51.06 | 0.04 |
| USA300HOU_1553 | rpmG3 | Ribosomal protein L33 | Cys36[a] | B | 6.6 | **9.46** | 5.76 | 0.10 | 15.22 | 0.12 |
| USA300HOU_2218 | rpmJ | Ribosomal protein L36 | **Cys11[a] (-SSB)** | B | 4.5 | **16.93** | 21.38 | 0.17 | 38.32 | 0.11 |
| USA300HOU_2218 | rpmJ | Ribosomal protein L36 | Cys27[a] | B | 3.1 | **16.52** | 6.69 | 0.43 | 23.21 | 0.10 |
| **Transport and binding proteins** | | | | | | | | | | |
| USA300HOU_2553 | copZ[#] | Copper chaperone | Cys13[a] | B | 6.2 | **19.85** | 30.60 | 0.28 | 50.45 | 0.13 |
| USA300HOU_2553 | copZ[#] | Copper chaperone | Cys16[a] | B | 3.3 | **19.85** | 30.60 | 0.28 | 50.45 | 0.13 |
| **Energy metabolism (ATP synthesis, central carbon metabolism)** | | | | | | | | | | |
| Glycolysis | | | | | | | | | | |
| USA300HOU_0802 | gap | Glyceraldehyde-3-phosphate DH | **Cys151[a] (-SSB)** | B | 10.5 | **29.46** | 8.28 | 0.13 | 37.74 | 0.04 |
| USA300HOU_1685 | pfkA | 6-phosphofructokinase | Cys73[a] | B | 24.1 | **10.90** | 7.00 | 0.52 | 17.90 | 0.04 |
| USA300HOU_1685 | pfkA | 6-phosphofructokinase | Cys226 | B | 17.4 | **23.24** | 18.46 | 0.11 | 41.70 | 0.18 |
| USA300HOU_1685 | pfkA | 6-phosphofructokinase | Cys232 | B | 2.8 | **23.24** | 18.46 | 0.11 | 41.70 | 0.18 |
| USA300HOU_1684 | pykA | Pyruvate kinase | Cys266[a] | B | 1.7 | **10.52** | 11.24 | 0.31 | 21.76 | 0.11 |
| Fermentation | | | | | | | | | | |
| USA300HOU_0610 | adh | Alcohol DH | Cys34 | B | 4.1 | **25.18** | 11.02 | 0.35 | 36.20 | 0.28 |
| USA300HOU_0610 | adh | Alcohol DH | Cys37[a] | B | 2.3 | **25.18** | 11.02 | 0.35 | 36.20 | 0.28 |
| USA300HOU_2110 | aldA | Aldehyde DH | **Cys279[a] (-SSB)** | B | 1.4 | **26.29** | 11.14 | 0.14 | 37.43 | 0.06 |
| USA300HOU_2291 | fdhA | Formate DH alpha subunit | Cys386[a] | B | 15.8 | **13.68** | 47.82 | 0.07 | 61.50 | 0.09 |
| Tricarboxylic acid cycle | | | | | | | | | | |
| USA300HOU_2348 | mqo1 | Malate:quinone oxidoreductase | Cys97 | B | 7.6 | **20.95** | 18.56 | 0.51 | 39.50 | 0.12 |

(*continued*)

TABLE 2. (CONTINUED)

| *Locus tag* | *Gene name* | *Protein function* | *Cys* | *Buried/ Exposed* | *RSA (%)* | *% Diff NaOCl/Co* | *Mean % oxidation control* | *CV* | *Mean % oxidation NaOCl* | *CV* |
|---|---|---|---|---|---|---|---|---|---|---|
| Other energy metabolism | | | | | | | | | | |
| USA300HOU_0964 | nadK | NAD(+) kinase | Cys208[a] | B | 1.8 | **11.00** | 18.36 | 0.17 | 29.35 | 0.15 |
| USA300HOU_0563 | nagB | Glucosamine-6-phosphate deaminase | Cys239 | B | 3.9 | **16.40** | 9.49 | 0.07 | 25.89 | 0.11 |
| USA300HOU_0902 | ndh | NADH dehydrogenase | Cys199 | B | 2.6 | **10.23** | 15.39 | 0.19 | 25.62 | 0.08 |
| **Amino acid biosynthesis** | | | | | | | | | | |
| USA300HOU_1536 | gcvPB | Glycine DH (decarboxylating) subunit 2 | Cys80[a] | B | 4.0 | **20.24** | 7.86 | 0.81 | 28.10 | 0.48 |
| USA300HOU_1240 | glnA | Glutamate—ammonia ligase | Cys291 | B | 4.1 | **10.52** | 14.77 | 0.05 | 25.29 | 0.33 |
| **Fatty acid, phospholipid and sterol metabolism** | | | | | | | | | | |
| USA300HOU_0942 | fabH2 | 3-oxoacyl-[acyl-carrier-protein] synthase | Cys220 | B | 7.2 | **11.15** | 11.09 | 0.35 | 22.24 | 0.06 |
| **Nucleotide biosynthesis** | | | | | | | | | | |
| USA300HOU_0413 | guaB | Inosine-5′-monophosphate DH | Cys326 | B | 1.4 | **25.09** | 7.49 | 0.28 | 32.58 | 0.06 |
| USA300HOU_2115 | pyrG | CTP synthase | Cys439[a] | B | 2.1 | **12.29** | 8.25 | 0.47 | 20.54 | 0.09 |
| USA300HOU_2265 | USA300HOU_2265 | Inosine-adenosine-guanosine-nucleoside hydrolase | Cys284 | B | 10.8 | **24.99** | 8.80 | 0.43 | 33.79 | 0.14 |
| **Biosynthesis of cofactors, prosthetic groups, and carriers** | | | | | | | | | | |
| USA300HOU_0929 | cdr | Coenzyme A disulfide reductase | Cys16[a] | B | 2.1 | **12.44** | 9.59 | 0.26 | 22.03 | 0.79 |
| USA300HOU_0561 | bshB2 | Bacillithiol biosynthesis deacetylase | Cys72[a] | B | 7.3 | **3.39** | 10.81 | 0.02 | 14.19 | 0.14 |
| USA300HOU_1417 | ypdA | Putative bacillithiol disulfide reductase | Cys14[a] | B | 5.9 | **3.20** | 8.39 | 0.58 | 11.59 | 0.08 |
| USA300HOU_1365 | brxB | Bacilliredoxin, YphP/YqiW family | Cys144[a] | B | 14.7 | **7.39** | 17.90 | 0.32 | 25.29 | 0.28 |
| USA300HOU_1824 | hemH | Ferrochelatase | Cys276 | B | 2.9 | **12.51** | 14.25 | 0.38 | 26.76 | 0.05 |
| USA300HOU_0873 | nifS | SufS subfamily cysteine desulfurase | Cys371[a] | B | 3.4 | **20.64** | 26.61 | 0.31 | 47.25 | 0.15 |
| USA300HOU_0874 | nifU | Iron–sulfur (Fe-S) cluster formation protein IscU | Cys41[a] | B | 11.1 | **26.30** | 17.85 | 0.09 | 44.15 | 0.15 |
| USA300HOU_0875 | sufB | Iron–sulfur (Fe-S) cluster formation protein SufB | Cys302 | B | 3.7 | **6.48** | 13.74 | 0.19 | 20.22 | 0.08 |
| USA300HOU_2257 | moaB | Molybdopterin cofactor biosynthesis protein MoaB | Cys34 | B | 20.8 | **13.81** | 9.42 | 0.06 | 23.23 | 0.13 |

Quantification of 58 Cys peptides with reversible thiol-oxidations in *S. aureus* USA300 that showed >10% increased oxidation under NaOCl stress using the OxICAT method. *S. aureus* USA300 was harvested before (control) and 30 min after exposure to 150 $\mu M$ NaOCl. Reduced and reversibly oxidized Cys residues were labeled with light and heavy ICAT reagents, respectively, using the OxICAT method. Quantification of % thiol oxidation was performed using the MaxQuant software (http://141.61.102.17/maxquant_doku/doku.php?id=start&#maxquant). The table includes locus tags, protein names, functions, Cys peptide sequences, surface access abilities, and % oxidation of the Cys residues under control and NaOCl stress conditions. Conserved Cys and their functions were marked with [a] and identified by searching the Conserved Domain Database (CDD) (www.ncbi.nlm.nih.gov/Structure/cdd/wrpsb.cgi). *S*-bacillithiolated Cys residues are marked with (+BSH) that are listed in Supplementary Figure S1. Cys functions were identified from the CDD and UniprotKB database and predicted proteins with redox-sensitive Cys residues are marked with # that were identified using the THIOREDOXOME database (http://gladyshevlab.org/THIOREDOXOME/tdb.html).The relative surface accessibility (RSA) for buried (B) or exposed (E) Cys residues was calculated using the NetSurfP ver. 1.1 (www.cbs.dtu.dk/services/NetSurfP/). The % thiol oxidation of each identified Cys peptide was calculated using the intensity values provided by MaxQuant software. Based on the % thiol oxidation of each Cys under control and NaOCl stress conditions, the % oxidation increase under NaOCl treatment was then calculated for each experiment. The CV is calculated as relative variability that equals the standard deviation divided by the mean of biological replicates for control and NaOCl stress samples, respectively. NaOCl-sensitive peptides with >10% increased thiol oxidation under NaOCl stress are highlighted using a gray shading gradient.

BSH, bacillithiol; CV, coefficient of variation; NADH, nicotinamide adenine dinucleotide; ICAT, isotope-coded affinity tag; RSA, relative surface accessibility; DH, dehydrogenase.

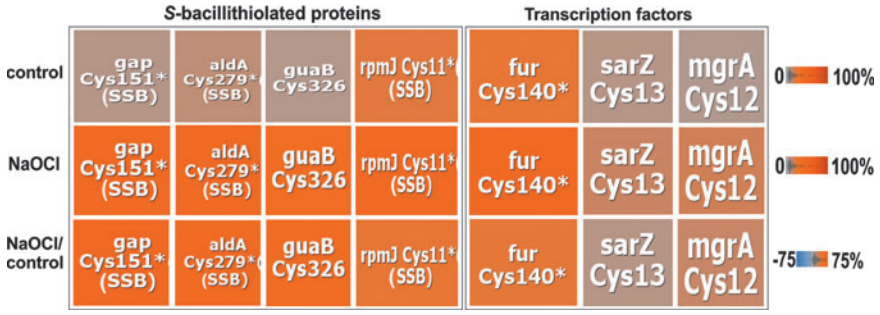


**FIG. 2. Close-ups of the redox treemaps of *S. aureus* USA300 showing *S*-bacillithiolated enzymes and redox regulators (SarZ, MgrA, and Fur).** Enlarged sections of the redox treemaps are shown that include the identified *S*-bacillithiolated proteins (Gap, AldA, GuaB, RpmJ) and NaOCl-sensitive redox-sensing regulators (MgrA, SarZ, and Fur). The close-ups show the percentages of thiol oxidation under control, NaOCl stress, and the percentage of oxidation change under NaOCl stress versus control as revealed in Figure 1 using the same color gradient. The symbol * denotes conserved Cys.

catalytic active sites at Cys151 and Cys279, respectively. Furthermore, the IMP dehydrogenase GuaB and the purine nucleosidase USA300HOU_2265 both displayed 25% increased oxidation under NaOCl stress (Tables 2; Supplementary Table S1).

Among the cell wall biosynthesis enzymes, the alanine racemase Alr2 (USA300HOU_2065) and the UDP-N-acetylglucosamine 1-carboxyvinyltransferase MurZ (USA 300HOU_2112) were identified as NaOCl-sensitive proteins. The glucose-inhibited division protein MnmG showed 20.8% increased oxidation under NaOCl stress. Many aminoacyl-tRNA synthetases were strongly oxidized under NaOCl stress. We detected 18–24% higher oxidation levels for the histidine- and phenylalanine tRNA ligases (HisS and PheT2) and for the queuine tRNA ribosyltransferase (Tgt) under NaOCl stress.

### *Five* S*-bacillithiolated proteins were identified using shotgun proteomics in* S. aureus*, including the glycolytic Gap as major target*

We used the previously applied shotgun proteomic approach for identification of *S*-bacillithiolated proteins under nonreducing conditions based on the 396 Da mass increase at Cys residues (16). Five *S*-bacillithiolated proteins were identified in NaOCl-treated cells of *S. aureus* USA300, including Gap, AldA, GuaB, RpmJ, and the manganese-dependent inorganic pyrophosphatase PpaC (Table 3; Supplementary Fig. S1). GuaB was *S*-bacillithiolated at its active site Cys307, which forms the thioimidate intermediate with the substrate and is *S*-thiolated also in other gram-positive bacteria (Table 3; Supplementary Fig. S1).

Gap and AldA were *S*-bacillithiolated at their catalytic active sites at Cys151 and Cys279, respectively (Fig. 2 and Table 3; Supplementary Fig. S1). The AldA homolog of *S. carnosus* was previously found *S*-bacillithiolated at Cys279 (16). The active site Cys of Gap is a conserved target for *S*-glutathionylation in eukaryotic Gap homologs. Cys151 of Gap showed 29.5% oxidation increase under NaOCl stress in the OxICAT analysis, which is reflected also by the mass spectra of the ICAT-labeled Cys151-peptides (Fig. 4A). Nonreducing BSH-specific Western blots further identified that Gap is the most abundant *S*-bacillithiolated protein under hypochlorite stress based on the size and supported by the MS results (Fig. 4B; Supplementary Fig. S1). Gap-SSB was detected in the *S. aureus* USA300 and COL strains, but is absent in the *bshA* mutant as expected.

### *Gap contributes as most abundant Cys protein with 4% to the total Cys proteome*

We were further interested in the contribution of Gap and other *S*-bacillithiolated proteins to the total Cys proteome of *S. aureus*. *S. aureus* USA300 encodes for 2694 proteins. These include 1864 proteins with 4935 Cys residues, indicating that the Cys content is 0.64% in the theoretical proteome (Supplementary Fig. S2A, B). Using shotgun proteomics, the spectral protein abundance for 600 proteins,

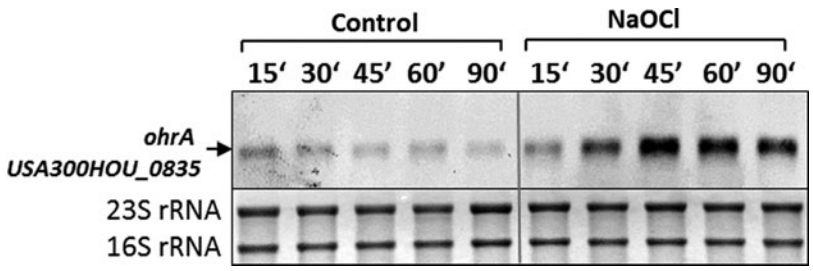


**FIG. 3. Northern blot analysis showing transcriptional induction of the SarZ-regulated *ohrA* gene (USA300-HOU_0835) under NaOCl stress.** RNA was isolated from *S. aureus* USA300 grown in Belitsky minimal medium under control and NaOCl stress conditions and subjected to Northern blot analysis for *ohrA* (*USA300HOU_0835)* transcription. Transcription of *ohrA* is upregulated due to SarZ thiol oxidation and inactivation under NaOCl stress as revealed by OxICAT analysis *in vivo*.

TABLE 3. IDENTIFICATION OF THE *S*-BACILLITHIOLATED GAP, ALDA, PPAC, RPMJ, AND GUAB IN *STAPHYLOCOCCUS AUREUS* USA300 USING SHOTGUN LC-MS/MS ANALYSIS

| *Protein* | *Accession* | *Function* | *Cys-SSB peptides* | *Prob (%)* | *SEQUEST XCorr* | *SEQUEST ΔCn* | *Cys-Mod.* | *Observed mass* | *Actual mass* | *Charge* | *ΔDa* | *ΔPPM* |
|---|---|---|---|---|---|---|---|---|---|---|---|---|
| Gap | A8Z1A0_STAAT | Glyceraldehyde-3-phosphate dehydrogenase | (K)TIVFNTNHQELDG SETVVSGASC**151** **(+BSH)**TTNSLAP VAK(V) | 99 | 4.8813 | 0.7119 | (+396) | 1.262.92 | 3.785.73 | 3 | 0.00989 | 2.6 |
| AldA | A8YY87_STAAT | Aldehyde dehydrogenase | (K)VVNNTGQVC**279** **(+BSH)**TAGTR(V) | 99 | 2.9038 | 0.7827 | (+396) | 605.9328 | 1.814.78 | 3 | –0.00041 | –0.2 |
| PpaC | PPAC_STAAT | Mn-dependent inorganic pyrophosphatase | (R)IANFETAGPLC **110(+BSH)**YR(A) | 99 | 3.2907 | 0.6747 | (+396) | 925.9006 | 1.849.79 | 2 | 0.00081 | 0.4 |
| RpmJ | RL36_STAAT | 50S ribosomal protein L36 | (K)VRPSVKPIC**11** **(+BSH)**EK(C) | 99 | 2.0458 | 0.5926 | (+396) | 826.4047 | 1.650.79 | 2 | –0.00051 | –0.3 |
| GuaB | A8Z0R0_STAAT | Inosine-5′-monophosphate dehydrogenase | (K)VGIGPGSIC**307** **(+BSH)**TTR(V) | 99 | 2.2835 | 0.6759 | (+396) | 778.8504 | 1.555.69 | 2 | 0.00077 | 0.5 |

Identification of *S*-bacillithiolated peptides in the *S. aureus* USA300 wild type using shotgun LC-MS/MS analysis and their Sequest Xcorrs, ΔCn scores, and mass deviations. The *S. aureus* USA300 wild type was exposed to 150 $\mu M$ NaOCl for 30 min and *S*-bacillithiolated proteins were identified using shotgun LC-MS/MS analysis and the Scaffold proteome software based on the mass increase of 396 Da (+BSH) at Cys peptides. The table lists the Uniprot accession number, protein name, function and molecular weight, the *S*-bacillithiolated Cys peptide sequence, and the quality control criteria for the peptide-SSB as obtained from the LC-MS/MS analysis and the Scaffold software (Xcorr, ΔCn scores, mass deviations Δppm, and ΔDa, observed and theoretical peptide masses, and charges of the modified peptide).

The *S*-bacillithiolated Cys is shown in ***bold-faced.***

LC-MS/MS, liquid chromatography tandem mass spectry.

including 398 Cys-containing proteins, was determined in the proteome of *S. aureus* USA300 (Supplementary Table S2 and Supplementary Fig. S2C). The protein abundance in the proteome is visualized using Voronoi treemaps (Fig. 5). The cell size corresponds to the spectral protein abundance and the color code denotes the numbers of Cys residues. The majority of 226 Cys proteins identified in the proteome possess only 1–2 Cys residues. However, there are also six proteins with >10 Cys residues. The most Cys-rich protein was identified as the formate dehydrogenase FdhA that contains 26 Cys residues coordinating several FeS clusters. Based on their spectral abundance, we identified 50 abundant Cys-containing proteins that contribute to 60% of the total *S. aureus* Cys proteome (Supplementary Fig. S2C). The redox state for the majority of these Cys peptides was quantified using the OxICAT approach (Supplementary Table S1). The Cys abundance treemap also shows that many ribosomal proteins and the pyruvate dehydrogenase do not possess Cys residues (Fig. 5).

The *S*-bacillithiolated Gap was identified among the most abundant Cys-containing proteins and contributes with 4% of the total Cys proteome (Supplementary Fig. S2C). This indicates that Gap makes the major contribution to the *S*-bacillithiolome of *S. aureus* as visualized also by the BSH Western blots. The other *S*-bacillithiolated proteins, AldA, RpmJ, GuaB, and PpaC, are less abundant and make with 0.1–0.7% of Cys abundance only a minor contribution to the total Cys proteome (Supplementary Table S2).

### *$H_2O_2$ and NaOCl-induced inactivation pathways of Gap in* S. aureus *due to overoxidation and* S*-bacillithiolation* in vitro

The active site of Gap is usually present in a highly conserved CTTNC motif in different organisms (Supplementary Fig. S3). However, in the *S. aureus* Gap, the second cysteine is replaced by a serine. The identification of *S*-bacillithiolated Gap under hypochlorite stress was intriguing since a previous proteomic study has shown that Gap of *S. aureus* is very sensitive to overoxidation to the sulfonic acid form in the presence of 100 m$M$ $H_2O_2$ *in vivo* (73). In another proteomic study, Gap was identified as reversibly oxidized by 10 m$M$ $H_2O_2$ in *S. aureus* (19). Thus, we were interested to study the inhibition of Gap activity *in vitro* due to overoxidation and *S*-bacillithiolation under both $H_2O_2$ and NaOCl stresses.

Gap of *S. aureus* was purified as His-tagged protein from *E. coli*. The inhibition of Gap activity by increasing $H_2O_2$ concentrations was monitored spectrophotometrically with G3P as substrate in the presence of $NAD^+$. The remaining Gap activity was determined by nicotinamide adenine dinucleotide (NADH) generation as absorbance change at 340 nm during the slope in the reaction, as described previously (61). Treatment of Gap with 100 $\mu M$ $H_2O_2$ leads to a 50% decrease in Gap activity, while exposure to 1–10 m$M$ $H_2O_2$ resulted in complete enzyme inactivation (Fig. 6A). Inactivation of Gap with 1–10 m$M$ $H_2O_2$ alone was irreversible due to overoxidation since Gap activity could be not restored with 10 m$M$ dithiothreitol (DTT) (Fig. 6C). To investigate whether *S*-bacillithiolation can protect the enzyme against irreversible overoxidation, Gap was pretreated with 10-fold molar excess of BSH before $H_2O_2$ exposure. Gap activity was already 90% inhibited after oxidation with 100 $\mu M$ $H_2O_2$ in the presence of

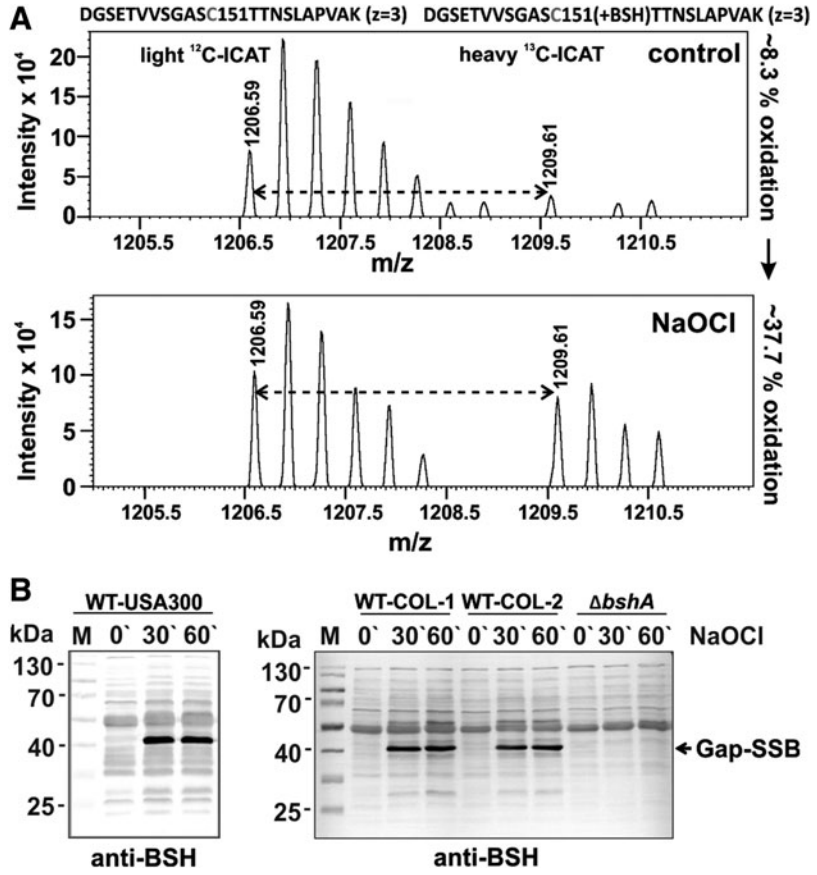


**FIG. 4. OxICAT analysis revealed a 29% increased oxidation of the Gap Cys151 peptide (A) and Gap was identified as most abundant *S*-bacillithiolated protein in *S. aureus* under NaOCl stress as shown by BSH-specific Western blot analysis (B). (A)** The OxICAT mass spectrometry results are shown for the Gap Cys151 peptide in *S. aureus* USA300 under control and 30 min after NaOCl stress. The reduced Gap Cys151 peptides in the cell extract are labeled with light $^{12}$C-ICAT, followed by reduction of all reversible thiol oxidation, including the *S*-bacillithiolated Cys151 peptides and subsequent labeling of previously oxidized Cys151 peptide by heavy $^{13}$C-ICAT reagent. According to the quantification by the MaxQuant software, the Cys151 peptide was 8.3% oxidized in the control and its oxidation level increased to 37.7% under NaOCl stress. **(B)** Nonreducing BSH-specific Western blot analysis identified Gap as most abundant *S*-bacillithiolated protein in *S. aureus* USA300 and COL strains under NaOCl stress. Two independent biological replicates are shown for *S. aureus* COL denoted as COL-1 and COL-2. Gap is *S*-bacillithiolated at the active site Cys151 under NaOCl stress as revealed by subsequent LC-MS/MS analysis (Supplementary Fig. S1A). BSH, bacillithiol; LC-MS/MS, liquid chromatography tandem mass spectry.

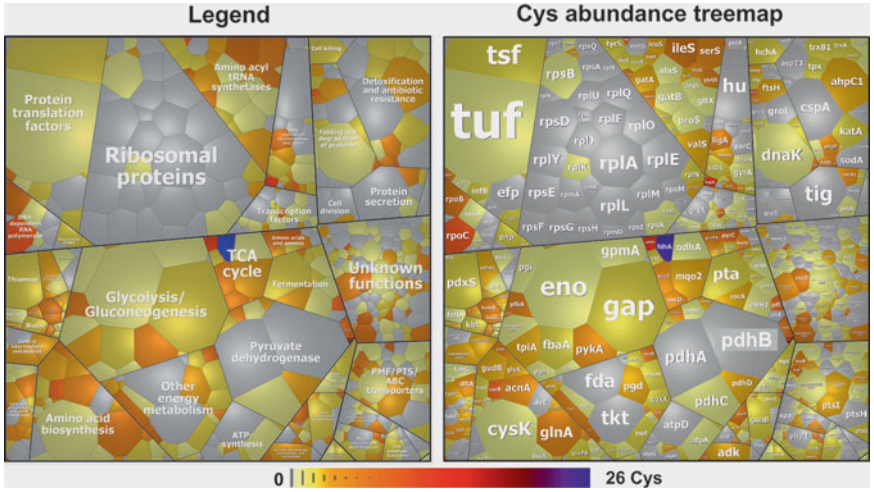


**FIG. 5. Voronoi treemaps visualize Gap as the most abundant Cys protein in the total Cys proteome of *S. aureus* USA300.** The treemap legend *(left)* indicates the classification of the *S. aureus* USA300 proteome into functional categories according to TIGRfam annotations. The cell size corresponds to the spectral counts of each protein identified in the proteome of *S. aureus* USA300 and classified according to TIGRfam. The Cys-containing proteins are color coded using a *yellow–red* color gradient based on their numbers of Cys residues (Supplementary Table S2). Proteins without Cys residues are displayed in *gray*.

BSH, while treatment with 100 $\mu M$ $H_2O_2$ alone only led to 50% decreased activity (Fig. 6A, B). Gap inactivation with $H_2O_2$ and BSH was caused by reversible *S*-bacillithiolation since DTT reduction resulted in recovery of Gap activity (Fig. 6C–E; Supplementary Fig. S9). These results support that the Gap active site is highly sensitive to overoxidation, which can be prevented by *S*-bacillithiolation in the presence of $H_2O_2$ and BSH.

Next, we determined the time-dependent Gap inactivation by both $H_2O_2$-dependent oxidation pathways (Supplementary Fig. S4). Gap was treated with 1 m$M$ $H_2O_2$ on ice with or without BSH and the remaining Gap activity was determined after different times of $H_2O_2$-dependent overoxidation and *S*-bacillithiolation. The Gap activity assays revealed that both *S*-bacillithiolation and overoxidation lead to 80% enzyme inhibition after 7.5 min of $H_2O_2$ treatment (Supplementary Fig. S4A). In addition, we analyzed the time course for the detection of Gap-SSB or the overoxidized Cys151 under $H_2O_2$ treatment with or without BSH using BSH-specific Western

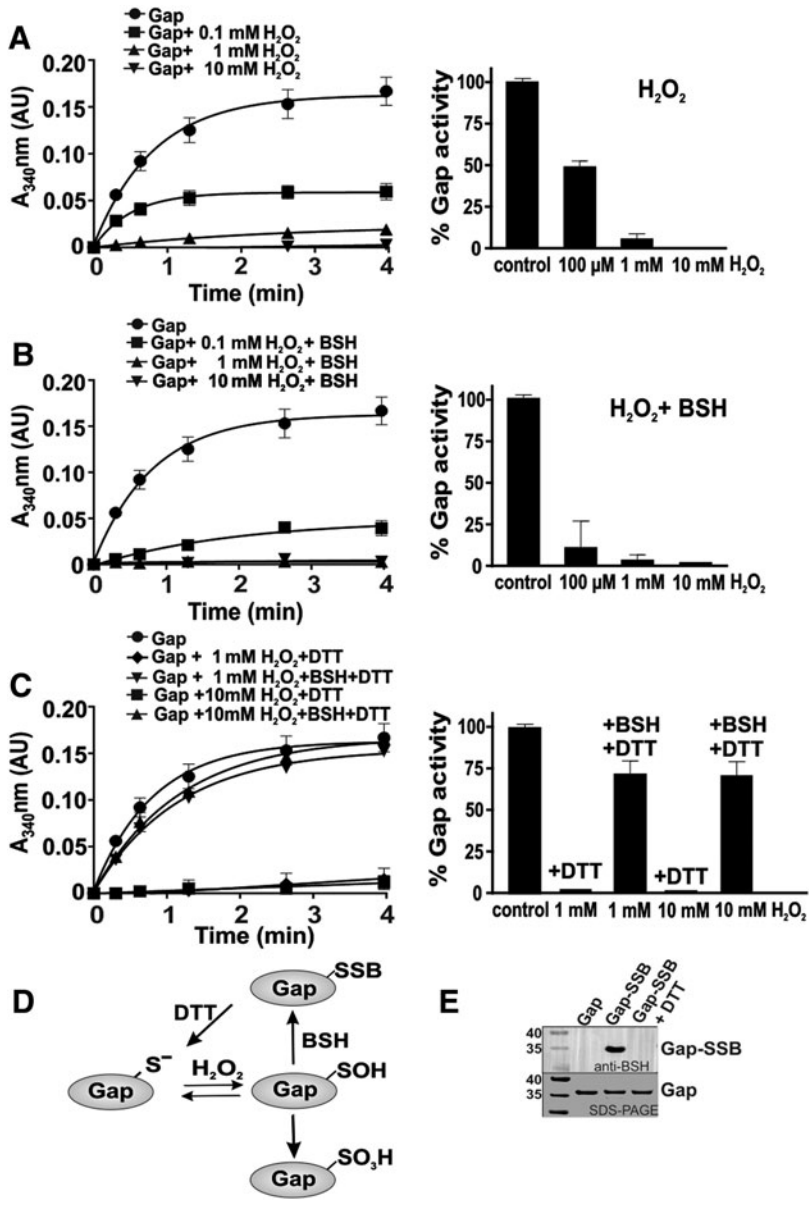


**FIG. 6. Inactivation of Gap of *S. aureus* in response to $H_2O_2$ *in vitro*.** **(A, B)** Reduced Gap (40 $\mu M$) was oxidized with 100 $\mu M$, 1, and 10 m$M$ $H_2O_2$ for 5 min in the absence **(A)** or presence of 10-molar excess of BSH (400 $\mu M$) **(B)** in reaction buffer (100 m$M$ Tris HCl, 1.35 m$M$ EDTA, pH 8.0). The remaining Gap activity was measured in the presence of G3P and $NAD^+$ spectrophotometrically, following NADH production at 340 nm. The Gap activity was calculated as absorbance change from the slope of the reaction in the first 80 s, as described in the Materials and Methods section. **(C)** To assess the reversibility of Gap inactivation by $H_2O_2$, Gap was treated with 1 and 10 m$M$ $H_2O_2$ alone or with $H_2O_2$ and BSH, followed by reduction with 10 m$M$ DTT. **(D)** Schematic showing the irreversible inhibition of Gap activity due to overoxidation of the active site Cys with $H_2O_2$ alone, while Gap activity was reversibly inhibited with $H_2O_2$ and BSH due to *S*-bacillithiolation. **(E)** *S*-bacillithiolation of Gap in the presence of 10 m$M$ $H_2O_2$ and BSH was confirmed using a BSH-specific Western blot analysis before and after subsequent DTT reduction. DTT, dithiothreitol; EDTA, ethylenediaminetetraacetic acid; G3P, glyceraldehyde-3-phosphate; $H_2O_2$, hydrogen peroxide.

blots or MS, respectively. The MS results identified the overoxidized Cys151 sulfonic acid (Cys151-$SO_3H$) after 1 min of $H_2O_2$ treatment (Supplementary Fig. S5). The *S*-bacillithiolated Gap could be also detected after 1 min of treatment with BSH and $H_2O_2$ (Supplementary Figs. S4B and S9). These results suggest that overoxidation and *S*-bacillithiolation occur at similar rates under $H_2O_2$ treatment *in vitro*. However, the Gap activity assays after treatment with different $H_2O_2$ concentrations indicate that Gap inhibition is faster with 100 $\mu M$ $H_2O_2$ in the presence of BSH compared with 100 $\mu M$ $H_2O_2$ alone, which only leads to 50% enzyme inhibition (Fig. 6A, B). Thus, *S*-bacillithiolation of Cys151 by $H_2O_2$ in the presence of BSH serves to protect the active site against overoxidation.

Since *S*-bacillithiolation of Gap was observed under NaOCl stress *in vivo*, we studied the dose-dependent Gap inactivation by NaOCl with or without prior exposure to BSH (Fig. 7). Treatment of Gap with 100–500 $\mu M$ NaOCl led to 50–75% inhibition of Gap activity. Pretreatment of Gap with BSH before exposure to 100 $\mu M$ NaOCl resulted in 70% activity decrease. Gap was fully inactivated with 1 m*M* NaOCl in the absence or presence of BSH. Treatment of Gap with 1 m*M* NaOCl alone resulted in irreversible inactivation due to overoxidation since Gap activity could be not restored using DTT. In the presence of BSH, Gap inactivation by NaOCl was caused by reversible *S*-bacillithiolation since 85% Gap activity could be restored by DTT reduction (Fig. 7C, D). Next, we studied the time course for NaOCl-induced overoxidation and *S*-bacillithiolation pathways in the presence of 1 m*M* NaOCl. The Gap activity assays with or without BSH showed that Gap inhibition is faster with BSH and NaOCl compared with NaOCl alone (Supplementary Fig. S6). These results indicate that *S*-bacillithiolation can efficiently prevent overoxidation of the Gap active site under NaOCl *in vitro*, supporting our *in vivo* finding.

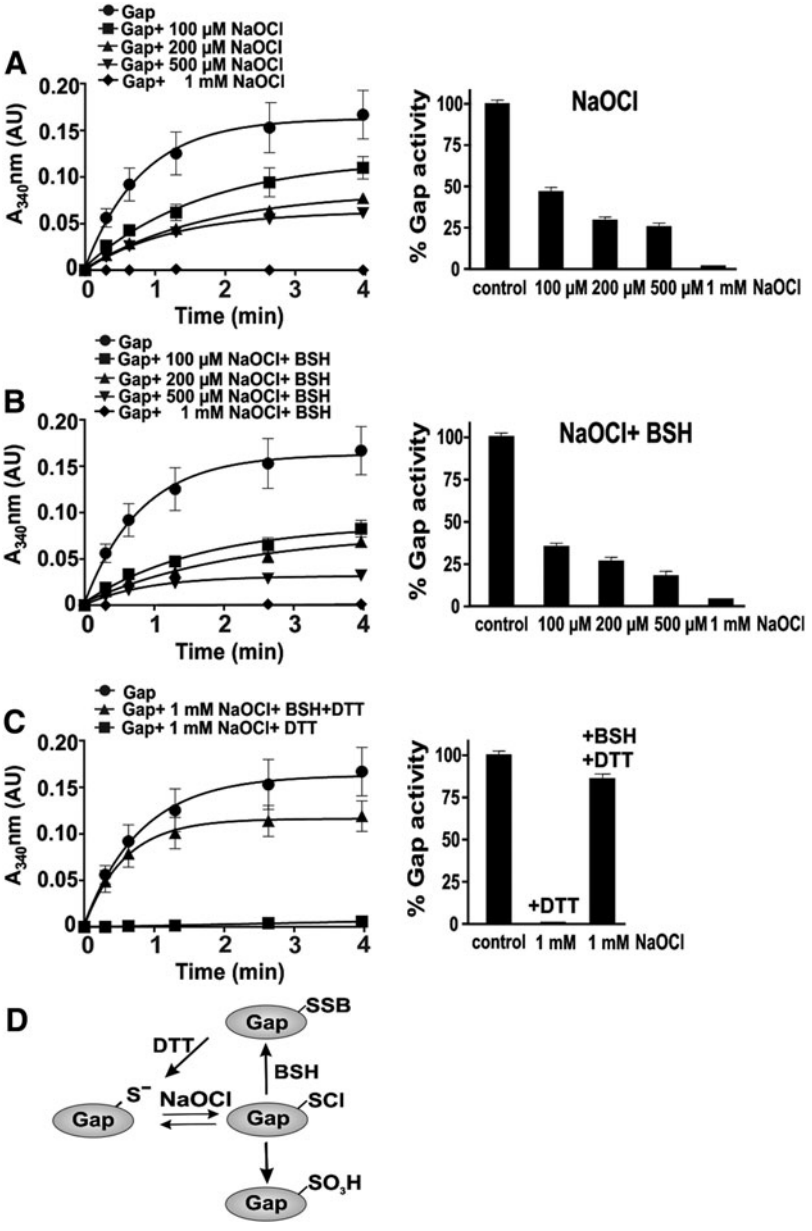


**FIG. 7. Inactivation of Gap of *S. aureus* in response to NaOCl *in vitro*.** **(A, B)** Reduced Gap was treated with 0.1–1 m*M* NaOCl for 5 min without **(A)** or with 10-molar excess of BSH **(B)** in reaction buffer (100 m*M* Tris HCl, 1.35 m*M* EDTA, pH 8.0). The remaining Gap activity was measured spectrophotometrically, following NADH production at 340 nm. The Gap activity was calculated as absorbance change from the slope of the reaction in the first 80 s, as described in the Materials and Methods section. **(C)** To analyze the reversibility of Gap inactivation by NaOCl, Gap was inactivated with 1 m*M* NaOCl in the absence or presence of BSH, followed by DTT reduction. Gap activity was irreversibly inhibited after treatment with NaOCl due to overoxidation since Gap activity could be not restored by DTT. In the presence of NaOCl and BSH, Gap was reversibly inactivated due to *S*-bacillithiolation since DTT reduction resulted in 85% recovery of Gap activity. **(D)** Schematic showing that NaOCl leads to the transient sulfenylchloride formation as unstable intermediate that reacts further with BSH to form *S*-bacillithiolated Gap. In the absence of BSH, Gap-SCl is quickly overoxidized resulting in irreversible inhibition of Gap activity *in vitro*.

### *Regeneration of* S*-bacillithiolated Gap using the bacilliredoxin Brx (SAUSA300_1321)* in vitro

The reversal of *S*-bacillithiolation was shown to require the glutaredoxin-like bacilliredoxins, YphP (BrxA) and YqiW (BrxB), in *B. subtilis* (24). Using a Brx-roGFP2 biosensor, we demonstrated recently that the YphP homolog of *S. aureus* (SAUSA300_1321 or Brx) is highly specific as bacilliredoxin to recognize BSSB (51). Thus, Gap activity was measured after debacillithiolation of Gap-SSB with Brx and Brx Cys mutant proteins (BrxCGA, BrxAGC) and G3P oxidation was followed by NADH production as absorbance change at 340 nm (Fig. 8A). Gap activity could be restored to 70% and 60% during debacillithiolation with Brx and the BrxCGA resolving Cys mutant *in vitro*, respectively. However, Gap activity was only 25% recovered with the BrxAGC active site mutant protein supporting the specificity of the Brx active site for the attack of BSH mixed disulfide. Debacillithiolation of Gap-SSB by Brx and the BrxCGA mutant was verified in BSH-specific Western blots (Fig. 8B; Supplementary Fig. S9). These results indicate that *S*-bacillithiolation of Gap functions in protection and redox regulation of the active site Cys and can be reversed by the bacilliredoxin Brx *in vitro* (Fig. 8C).

### *Structural features of the Gap active site during overoxidation and* S*-bacillithiolation*

We were interested in structural changes of Gap after overoxidation and *S*-bacillithiolation. The crystals of $H_2O_2$-treated overoxidized Gap diffracted X-rays to 2.6 Å resolution and belonged to the $P2_12_12_1$ space group. Previously, several crystal structures of the Gap holo- and apoenzyme have been reported with the protein always crystallized in the $P2_1$ space group (57). The structure of the overoxidized Gap contains four monomers in an asymmetric unit, each consisting of the $NAD^+$-binding domain (residues 1–150) and the

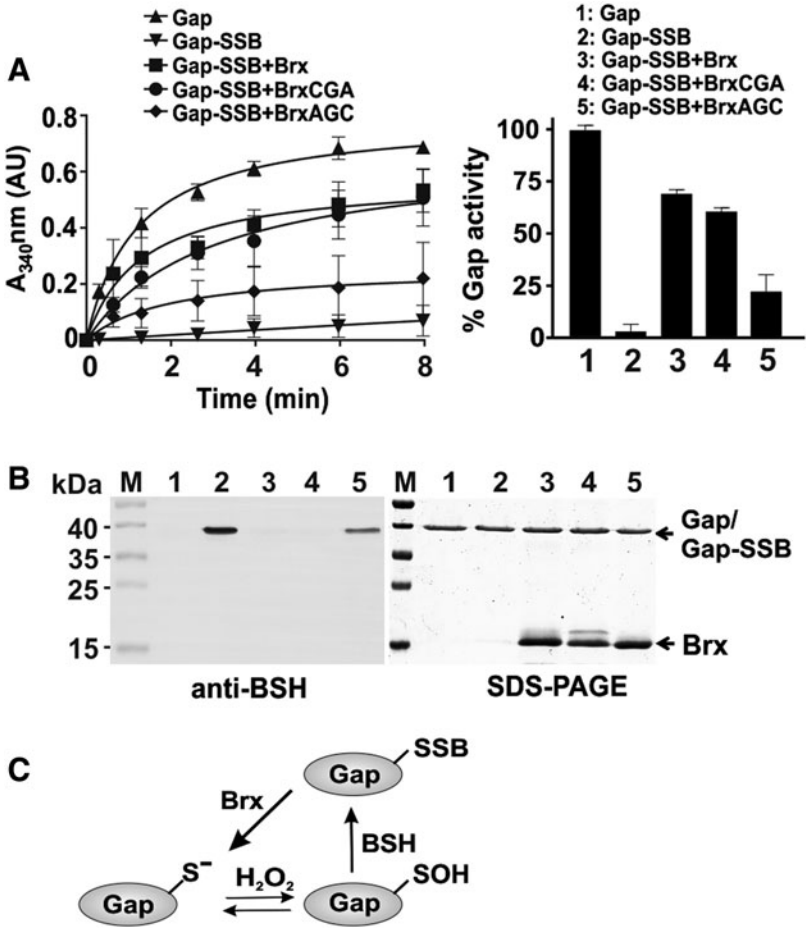


**FIG. 8. Recycling of *S*-bacillithiolated Gap requires the bacilliredoxin Brx *in vitro*.** **(A)** Gap activity is reversibly inhibited by *S*-bacillithiolation *in vitro* and can be restored by reduction using the bacilliredoxin Brx (SAUSA300_1321). Debacillithiolation required the Brx active site Cys. The BrxAGC mutant showed weak activity to reduce Gap-SSB, while the Brx resolving Cys mutant (BrxCGA) could restore Gap activity similar to the wild-type Brx protein. *S*-bacillithiolated Gap was generated *in vitro* by treatment of 25 $\mu M$ Gap with 2.5 m$M$ $H_2O_2$ in the presence of 250 $\mu M$ BSH. For debacillithiolation, 2.5 $\mu M$ Gap-SSB was incubated with 12.5 $\mu M$ Brx, BrxAGC, and BrxAGC proteins for 30 min. Gap activity was measured after addition of G3P and $NAD^+$ by spectrophotometric monitoring of NADH generation at 340 nm. **(B)** The level of debacillithiolation of Gap-SSB *in vitro* by Brx and BrxCys mutant proteins was monitored using nonreducing BSH-specific Western blot analysis. The SDS-PAGE is shown as loading control (*right*). The numbers 1–5 shown in the BSH Western blot and in the SDS-PAGE refer to the legend shown in **(A)**. **(C)** Schematic for the reduction of *S*-bacillithiolated Gap using the bacilliredoxin Brx. SDS-PAGE, sodium dodecyl sulfate–polyacrylamide gel electrophoresis.

catalytic domain (residues 151–336) (57) (Supplementary Fig. S7A). The overall fold of overoxidized Gap is almost identical to previously reported reduced Gap structures, with only slight conformational differences observed in the loop regions comprising residues 59–72, 75–90, and 111–118. The root-mean square deviation after global superposition of overoxidized Gap with the holo- (PDB code: 3LVF) or apoenzyme (PDB code: 3LC7) was 1.01 and 1.11 Å, respectively. Interestingly, during previous structural analyses, Gap always copurified with $NAD^+$, which had to be removed *via* activated charcoal to obtain the apoenzyme (57). In contrast, the present Gap structure does not contain $NAD^+$, thus representing an apo form of the enzyme. Thus, $H_2O_2$ treatment seems to have led to loss of the coenzyme.

According to our MS results and previous publications (73), the Gap sulfonic acid was identified by MS as overoxidized form. In the structure of overoxidized Gap, the sulfonic acid form could be modeled into the electron density of the active site Cys151 in each monomer (Supplementary Fig. S7B, C). Overoxidation of Cys151 results in enzyme inhibition as supported by our activity assays. During catalysis, the sulfhydryl group of Cys151 attacks the nucleophilic carbon of the G3P substrate to form a covalent intermediate, thiohemiacetal (72). In the active enzyme, His178 forms an ion pair with Cys151, which increases the acidity and nucleophilicity of the thiol group. During G3P oxidation, His178 hydrogen bonds with the acyl carbonyl of the substrate and stabilizes the hemithioacetal intermediate (57). Apart from interfering with the function of Cys151, the sulfonyl moiety of the hyperoxidized Cys151 also interacts with the main chain carbonyl of Asn316 and the imidazole ring of His178 (Fig. 9A; Supplementary Fig. S7D). Thus, hyperoxidation of Cys151 affects the function of two key catalytic residues of Gap, Cys151, and His178, leading to irreversible inactivation of the enzyme.

To obtain insights into the structural changes upon *S*-bacillithiolation, BSH was modeled into the active site of the

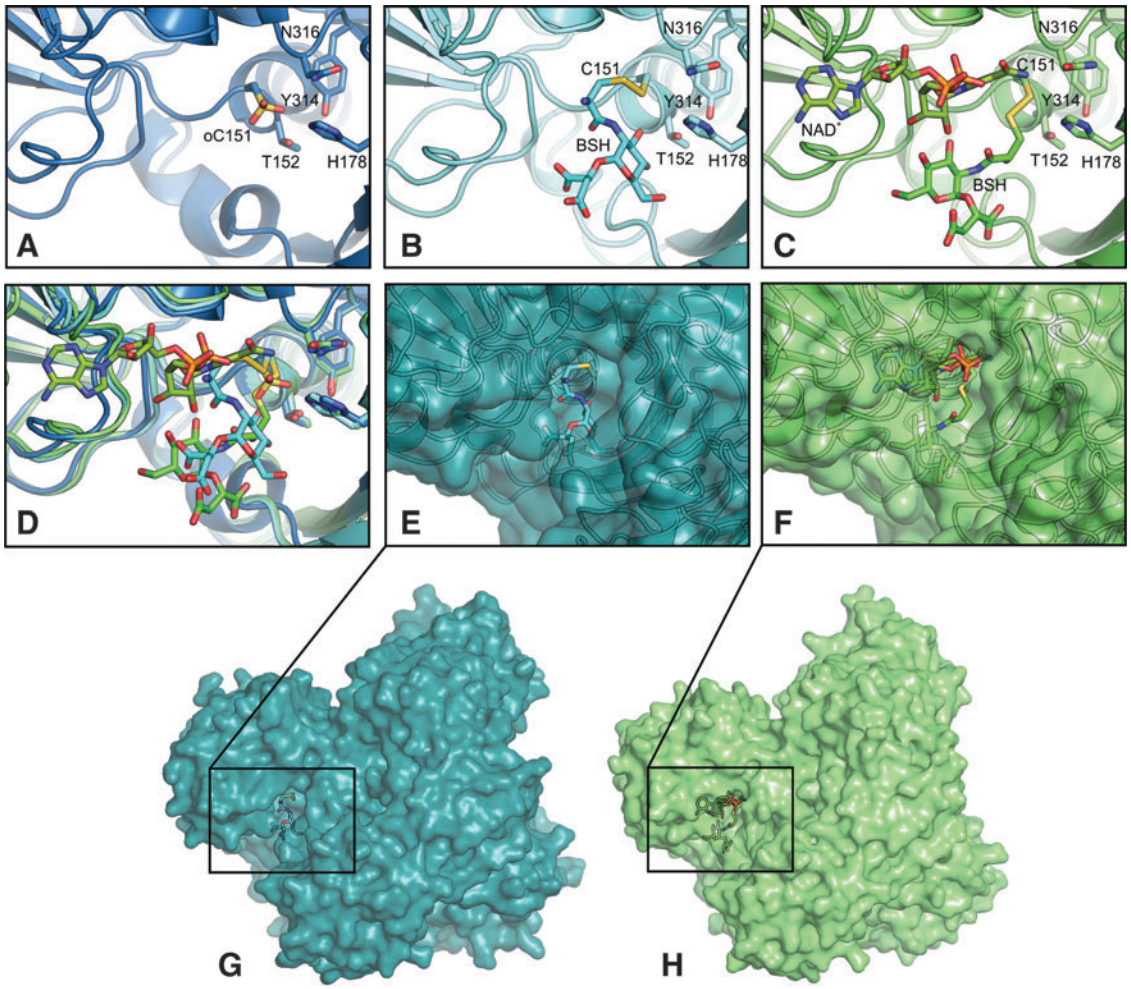


**FIG. 9. Structural insights into the Gap active site after overoxidation and *S*-bacillithiolation.** **(A)** Crystal structure of the overoxidized active site Cys151 (Cys-$SO_3H$, oC151) of Gap. **(B, C)** Computational model of BSH docked into the active site of the Gap apoenzyme **(B)** and holoenzyme with the $NAD^+$ coenzyme **(C)** using a covalent docking algorithm that takes into account the possibility of bond formation between ligand and receptor. Shown is the best pose of 10 best poses of the *S*-bacillithiolated active site. **(D)** Superposition of Gap-$SO_3H$ with the *S*-bacillithiolated apo- and holoenzyme active sites. **(E, F)** The *S*-bacillithiolated active site pocket of the apoenzyme **(E)** and holoenzyme **(F)** structures rotated by 25° over *y* axis in respect to **(B, C)**. **(G, H)** Surface representation of apoenzyme **(G)** and holoenzyme **(H)** with docked BSH.

apo- and holoenzyme structures using molecular docking (Fig. 9B, C). We used a covalent docking algorithm that takes into account the possibility of bond formation between ligand and receptor. Docking of BSH into the apo- or holoenzyme structure resulted in a set of covalent complexes (10 best poses), in which the disulfide bond can readily form and which are structurally very similar at least in the vicinity of the disulfide bond, suggesting a high confidence in the docking pose (Supplementary Fig. S8). In the holoenzyme structure, the $NAD^+$ cofactor partially occludes the binding pocket and narrows the space available for BSH binding. As a result, in the holo-Gap active site, where $NAD^+$ is present, BSH takes up conformations, which differ significantly less compared with the ones in the apoenzyme. When superimposing the two best binding poses, BSH in the apoenzyme structure partially occupies the part of the pocket where $NAD^+$ would be present (Fig. 9D). However, in both cases, *S*-bacillithiolation of the active site does not require major conformational changes of the protein (Fig. 9E–H). In addition, previous molecular dynamic simulations of human GAPDH (61) suggested little fluctuations of the protein. Taken together, we suggest that BSH can undergo disulfide formation with the active site at little energetic or entropic costs. This may further explain why Gap as the most abundant redox-sensitive protein in the proteome of *S. aureus* is also the most abundant *S*-bacillithiolated protein under NaOCl stress.

## Discussion

Dynamic thiol redox switches are the hallmarks of oxidative stress response and the major principle of redox signaling mechanism in prokaryotes and eukaryotes (33). Quantitative redox proteomic methods such as OxICAT allow to determine the redox state of proteins thiols and to dissect redox-sensitive thiols at high resolution (9, 48). To date, global thiol redox proteomics in the major pathogen *S. aureus* identified only few targets for oxidation under $H_2O_2$ stress (19, 77). However, *S. aureus* shows remarkable resistance to 100 m*M* $H_2O_2$, which is attributed to the constitutive expression of the catalase KatA indicating that *S. aureus* is well adapted to peroxide stress during infections (36).

In this study, we used OxICAT to monitor the redox state of 228 Cys residues in *S. aureus* USA300 under more severe infection-like conditions as provoked by hypochlorite. In untreated cells, the majority of thiols (84.6%) are reduced with an oxidation degree <25%, which is in agreement with previous studies in *E. coli* and yeast cells (9, 48). Under NaOCl stress, 58 NaOCl-sensitive proteins showed >10% increased oxidation, indicating that 25% of all identified protein thiols are redox sensitive in *S. aureus*. To analyze whether these NaOCl-sensitive Cys residues are buried or surface exposed, we calculated their relative surface accessibilities (RSAs) using NetSurfP (www.cbs.dtu.dk/services/NetSurfP/). However, only 9 of 228 Cys residues have RSA values of >30% and are predicted as solvent exposed (Table 2 and Supplementary Table S1). The RSA calculations clearly indicate that NaOCl-sensitive Cys residues are often the active site centers that are not surface exposed and buried in the predicted secondary protein structure.

Among the NaOCl-sensitive proteins with the highest oxidation increase of 20–30%, we identified Gap, AldA, and GuaB as *S*-bacillithiolated at their conserved substrate-binding active sites. Only a few *S*-bacillithiolated proteins were found by the shotgun proteomic approach due to the instability and low abundance of the BSH-modified peptides. Thus, we assume that many more NaOCl-sensitive proteins of our OxICAT dataset are modified by *S*-bacillithiolation, but failed to be identified using the shotgun method.

Apart from *S*-bacillithiolation, also alternative *S*-thiolations are possible in *S. aureus* under NaOCl stress such as S-cysteinylation or CoASH mixed disulfides since cysteine and CoASH are also present in the thiol metabolome of *S. aureus* (58, 64). Moreover, the Cdr displayed an increased oxidation level under NaOCl stress at its conserved Cys16 in our OxICAT analyses and was previously shown to function in reduction of CoASH disulfides in *S. aureus* (18, 55). However, *S*-cysteinylation and CoASH mixed disulfides were not detected by MS due to their low abundance or instability.

Many Zn-containing NaOCl-sensitive proteins were identified, such as the Fur repressor, which is oxidized in its Zn-binding site. Zn-binding sites are common redox switch motifs (37). The best-studied example is the oxidation-sensitive Hsp33 chaperone that responds to hypochlorite by a redox switch in its Zn motif and protects *E. coli* proteins against oxidative aggregation (26, 38, 46). NaOCl-sensitive Zn-containing proteins include the alcohol dehydrogenase Adh and the ribosomal proteins, RpmG3 and RpmJ. Several previously predicted redox-sensitive Cys residues are found in CxxC motifs, such as the copper chaperone, CopZ, and the antioxidant proteins, AhpC, TrxB, and ArsC (21). These results are in agreement with previous redox proteomic results in *E. coli* under NaOCl stress (48). Increased oxidation levels were detected for both MarR/OhrR family regulators MgrA and SarZ that are oxidized at their single Cys residues. Using Northern blot analyses, we confirmed that SarZ oxidation leads to derepression of transcription of the *ohrA* gene (*USA300-HOU_0835*) in *S. aureus*. Thus, the OxICAT approach identified increased oxidation of both major thiol redox regulators under NaOCl stress in *S. aureus*.

The most abundant *S*-bacillithiolated protein was the glycolytic Gap enzyme in *S. aureus* under NaOCl stress, which was *S*-bacillithiolated at the active site Cys151. Gap is the most abundant Cys-containing protein contributing 4% to the total Cys proteome. The active site Cys is used for the nucleophilic attack at the aldehyde group of the G3P substrate to catalyze the substrate-level phosphorylation of G3P to 1,3-bisphosphoglycerate with production of NADH (34). Gap homologs are common targets for oxidation in eukaryotes and prokaryotes and subject of different post-translational thiol modifications, including *S*-sulfenylation, *S*-glutathionylation, *S*-nitrosylation, and *S*-sulfhydration, resulting in reversible enzyme inactivation (10, 34). Inactivation of Gap has been shown to redirect the glycolytic flux into the pentose phosphate pathway to supply nicotinamide adenine dinucleotide phosphate (NADPH) as reducing power under oxidative stress (10, 66).

Gap of *S. aureus* was previously identified as oxidation-sensitive target for reversible thiol modification (19) and was also found to be overoxidized at its active site Cys151 under $H_2O_2$ stress (73). Using biochemistry, MS, and X-ray crystallography, we confirmed previous findings that the glycolytic Gap enzyme from *S. aureus* is highly sensitive to overoxidation to Cys sulfonic acid *in vitro* in the presence of $H_2O_2$ alone. In this work, we found that Gap is the most abundant *S*-bacillithiolated protein under NaOCl stress

*in vivo*. We further demonstrate that *S*-bacillithiolation functions in reversible inhibition of Gap activity under $H_2O_2$ and NaOCl treatment *in vitro* and protects the active site Cys against overoxidation to ensure fast regeneration of this essential glycolytic enzyme during recovery of cells. Our Gap activity assays suggest that both pathways, the overoxidation and *S*-bacillithiolation, operate at similar kinetics under $H_2O_2$ treatment, while inactivation due to *S*-bacillithiolation was faster under NaOCl stress. Together, our results confirm the preference for formation of *S*-thiolation in the presence of LMW thiols as observed in many eukaryotic Gap homologs (34, 43, 78).

The reactivity of the active site cysteine toward $H_2O_2$ and the substrate G3P was recently shown to depend on two different mechanisms (34, 61). The catalytic Cys is in close proximity with His178 in the structure of Gap of *S. aureus* that attracts the thiol proton, leading to deprotonation and increased acidity of the catalytic Cys. The acidic nature explains the reactivity of catalytic Cys toward the substrate G3P that covalently reacts with the nucleophilic thiolate during the catalytic cycle (34, 62). However, the increased acidity of Cys151 does not explain its strong reactivity toward $H_2O_2$. Instead, the reactivity of the active site thiolate depends on a specific $H_2O_2$-binding pocket, transition state stabilization, and a proton relay mechanism promoting leaving group departure (34, 61).

This proton relay mechanism also determines the preferred modification by *S*-bacillithiolation of Gap in *S. aureus* under $H_2O_2$ *in vitro*, which requires the initial formation of a sulfenic acid, followed by reaction to the BSH mixed disulfide. HOCl shows very fast reaction rates with thiols ($3\times10^7$ $M^{-1}s^{-1}$) that are several orders of magnitude higher compared with $H_2O_2$ (17, 27, 30, 60, 74). HOCl first leads to chlorination of thiols resulting in an unstable sulfenylchloride intermediate that reacts further to form disulfides in the presence of another thiol. In the absence of proximal thiols, the sulfenylchloride quickly leads to irreversible oxidation stages (17, 30, 52). We have shown in *S. aureus* that *S*-bacillithiolation functions in protection and redox regulation of the Gap active site against overoxidation under NaOCl stress *in vitro* and *in vivo*. Molecular docking of BSH into the active site of the Gap apo- and holoenzyme was used to model the *S*-bacillithiolated active site at high confidence. The model of Gap-SSB structure suggests that BSH can undergo disulfide formation with Cys151 without major conformational changes. This may explain why the most abundant Cys protein Gap is the preferred and dominant target for *S*-bacillithiolation inside *S. aureus* cells.

*S*-glutathionylation of the active site Cys of Gap was found in many eukaryotic organisms, such as *Arabidopsis thaliana*, the malaria parasite *Plasmodium falciparum*, or in human endothelial cells, leading to reversible inhibition of Gap activity (3, 43, 69). Reactivation of Gap was catalyzed by glutaredoxins and thioredoxins in plants and malaria parasites (3, 43). In *B. subtilis*, the bacilliredoxins, BrxA and BrxB, were shown to catalyze the reduction of *S*-bacillithiolated OhrR and MetE *in vitro* (24). In this study, we showed that *S*-bacillithiolated Gap is also a substrate for the bacilliredoxin Brx (SAUSA300_1321) in *S. aureus*, which requires the active site Cys for debacillithiolation *in vitro*. Thus, the bacilliredoxin pathway is also involved in regeneration of Gap activity in *S. aureus*.

## Materials and Methods

### *Bacterial strains and growth conditions*

Bacterial strains used were *S. aureus* COL and USA300 and its isogenic *bshA* mutants as described previously (64). For cloning and genetic manipulation, *E. coli* DH5a and BL21 (DE3) p*lysS* were cultivated in Luria Bertani (LB) medium. For NaOCl stress experiments, *S. aureus* USA300 and COL strains were cultivated in LB medium until an optical density at 540 nm ($OD_{540}$) of 2.0, transferred to Belitsky minimal medium, and treated with 150 $\mu M$ NaOCl stress as described (51). NaOCl, diamide, DTT, N-ethylmaleimide (NEM), and $H_2O_2$ (35% w/v) were purchased from Sigma-Aldrich.

### *MS-based thiol redox proteomics using the OxICAT approach*

*S. aureus* USA300 was harvested before and after exposure to 150 $\mu M$ NaOCl for 30 min, respectively. The OxICAT method was performed according to the protocol of Lindemann and Leichert (49) with the modification that cells were disrupted using a ribolyzer. The ICAT-labeled peptides were dissolved in 0.1% (v/v) acetic acid and loaded onto self-packed LC columns with 10 $\mu$l of buffer A (0.1% (v/v) acetic acid) at a constant pressure of 220 bar without trapping. Peptides were eluted using a nonlinear 85-min gradient from 1% to 99% buffer B (0.1% (v/v) acetic acid in acetonitrile) with a constant flow rate of 300 nl/min and measured using Orbitrap MS as described (6). The *S. aureus* USA300 sequence database was extracted from Uniprot and used by the search engine Andromeda and the MaxQuant software (version 1.5.1.2) to quantify the ICAT-labeled Cys peptides. Two miscleavages were allowed, the parent ion mass tolerance was 10 ppm and the fragment ion mass tolerance was 1.00 Da. The average percentage of oxidation of each Cys peptide and the percentage change under NaOCl stress were calculated from 2 to 3 biological replicates using the intensity values provided by MaxQuant. Voronoi treemaps were generated using the Paver software to visualize the percentage oxidation of all identified ICAT-labeled peptide pairs. The OxICAT proteomic data have been deposited to the ProteomeXchange Consortium *via* the PRIDE partner repository with the dataset identifier PXD004918.

### *Identification of* S*-bacillithiolated and overoxidized Cys peptides using LTQ-Orbitrap MS*

For identification of *S*-bacillithiolated peptides, NEM-alkylated protein extracts were prepared from *S. aureus* USA300 cells after exposure to 150 $\mu M$ NaOCl for 30 min as described (15). The protein extracts were separated by 15% nonreducing sodium dodecyl sulfate–polyacrylamide gel electrophoresis (SDS-PAGE), followed by tryptic in-gel digestion and LTQ-Orbitrap-Velos MS, as described (15). Post-translational thiol modifications of proteins were identified by searching all tandem mass spectrometry (MS/MS) spectra in dta format against the *S. aureus* USA300 target–decoy protein sequence database extracted from UniprotKB release 12.7 (UniProt Consortium, Nucleic acids research 2007, 35, D193-197) using Sorcerer™-SEQUEST® (Sequest v. 2.7 rev. 11, Thermo Electron, including Scaffold 4.0; Proteome Software, Inc., Portland, OR). The SEQUEST search parameters and thiol modifications were used as described (15).

The scores and mass deviations of the *S*-bacillithiolated peptides are shown in detail in Supplementary Figure S1, including their fragmentation spectrum and ion tables.

MS of the $H_2O_2$-treated overoxidized Gap was performed after in-gel tryptic digestion using nLC-MS/MS by Orbitrap fusion, as described previously (45). For Cys151-$SO_3H$ peptide identification and quantification, MS1 data were filtered to the precursor target masses applying an m/z window of 3 ppm. Isotopic distribution and fragmentation spectra were inspected manually in different charge states in successive MS2 scans in different overoxidized Gap samples.

### *Cloning, expression, and purification of the* S. aureus *Gap, Brx, and Brx Cys-Ala mutant proteins in* E. coli

The previously constructed plasmids, pET11b-Brx-roGFP2, pET11b-BrxAGC-roGFP2, and pET11b-BrxCGA-roGFP2 (51), were used as template to amplify *S. aureus brx* (*SAUSA300_1321*), *brx*AGC, and *brx*CGA by PCR using primer pairs 1321-roGFP2-For-NheI (5′-CTAGCTAGCATGAATGCATATGATGCTTATATGAAAG-3′) and roGFP2-1321-Rev-BamHI (5′-CGCGGATCCTTAGTGATGGTGATGGTGATGTTTACAATTT TCGTCAAAGGC-3′). The reverse primer also encodes the C-terminal $His_6$-tag. The PCR products were digested with *Nhe*I and *Bam*HI and inserted into plasmid pET11b (Novagen) that was digested using the same restriction enzymes to generate plasmids pET11b-*brx*, pET11b-*brxAGC*, and pET11b-*brxCGA*. The primer pairs gap-For-NdeI (5′-GGAATTCCATATGGCAGTAAAAGTAGCAATTAATG-3′) and gap-Rev-BamHI (5′-CGCGGATCCTTAGTGATGGTGATGGTGATGTTTAGAAAGTTCAGCTAAGTATGC-3′) were used to amplify the *S. aureus gap* gene (SAUSA300_0756) by PCR. Chromosomal DNA of *S. aureus* USA300 was used as template. The PCR products were digested with the restriction enzymes, *Nde*I and *Bam*HI, and inserted into plasmid pET11b that was digested with the same enzymes to generate plasmids pET11b-*gap*. The correct sequences of the cloned genes were confirmed by sequencing. The plasmids were transformed into *E. coli* BL21 (DE3) p*lysS* (Novagen).

For protein expression, *E. coli* BL21(DE3) plysS strains with the plasmids, pET11b-*gap*, pET11-*brx*, pET11b-*brxAGC*, and pET11b-*brxCGA*, were grown in 1 liter LB medium and 1 m*M* isopropyl-*β*-D-thiogalactopyranoside (IPTG) was added at the exponential phase (OD600 of 0.8) for 3 h at 37°C. His-tagged proteins were purified using His Trap™ HP Ni-NTA columns and the ÄKTA purifier liquid chromatography system (Amersham Bioscience). The proteins were further concentrated to 2–6 mg/ml using Amicon Ultra concentrators (Millipore). Before the activity assays, Gap and Brx proteins were reduced with 10 m*M* DTT for 30 min, followed by DTT removal using Micro Biospin 6 columns (Biorad).

### *Gap activity assay*

Gap activity was monitored spectrophotometrically at 340 nm and 25°C by the production of NADH. The oxidation of G3P to 1,3-bisphosphoglycerate (1,3-BPG) was measured in an assay mixture containing 1.25 m*M* $NAD^+$ and 0.25 $\mu M$ Gap in argon-flushed 20 m*M* Tris-HCl, pH 8.7, with 1.25 m*M* ethylenediaminetetraacetic acid and 15 m*M* sodium arsenate. After preincubation, the reaction was started by addition of 0.25 m*M* D,L-G3P. Sodium arsenate was used as a cosubstrate to form unstable 1-arseno-3-phosphoglycerate, as described previously (61). Degradation of the product allows a favorable equilibrium for measuring the rate of Gap activity in the glycolytic forward reaction. Initial rates were determined by calculation of the slope in the linear part of the curve during the first 80 seconds at the beginning of the reaction (linear regression function, GraphPad) as described previously (61). Percentage of Gap activity was calculated as ($Rate_{inactivated}/Rate_{untreated}$ x 100%). The results are presented as mean ± SEM from at least three separate experiments.

### S-*bacillithiolation of Gap* in vitro *and reduction by the bacilliredoxin Brx*

About 25 $\mu M$ of purified Gap was *S*-bacillithiolated with 250 $\mu M$ BSH in the presence of 2.5 m*M* $H_2O_2$ for 5 min. Excess of BSH and $H_2O_2$ was removed with Micro Biospin 6 columns (Biorad). For the Brx debacillithiolation assay, Gap-SSB was incubated with Brx, BrxCGA, and BrxAGC at 37°C for 30 min, followed by Gap activity assays and nonreducing BSH-specific Western blot analysis, as described (16).

### *Western blot analysis*

The *S*-bacillithiolated proteins were harvested from *S. aureus* USA300 wild-type and *bshA* mutant cells after exposure to 150 $\mu M$ NaOCl, separated by nonreducing SDS-PAGE, and subjected to BSH-specific Western blot analysis using the polyclonal rabbit anti-BSH antiserum, as described previously (16).

### *Northern blot experiments*

Northern blot analyses were performed as described before (15) using RNA isolated from *S. aureus* USA300 wild type under control conditions and after treatment with 150 $\mu M$ NaOCl. Hybridization specific for *ohrA* (*USA300HOU_0835*) was performed with the digoxigenin-labeled RNA probe synthesized *in vitro* using T7 RNA polymerase from T7 promoter containing internal PCR products using the primer pairs ohrA-for, 5′ TGGCAATACATTATGAAACTAAAGC 3′, and ohrA-T7-rev, 5′ CTAATACGACTCACTATAGGGAGATTTAAATCGACATTAATATTTCCTTGA 3′.

### *Crystallographic procedures*

Before crystallization, $H_2O_2$-treated overoxidized Gap was concentrated to 11 mg/ml. Crystals of overoxidized Gap were grown at 18°C using the hanging drop vapor diffusion technique and 30% (w/v) PEG 3350, 0.1 *M* Tris, pH 8.5, as the reservoir solution. Crystals were cryoprotected by transfer into mother liquor mixed with 50% (v/v) PEG 400 in a 1:1 ratio and flash-cooled in liquid nitrogen. X-ray diffraction data were collected from a single crystal at 100 K on beamline 14.1 of the BESSY II storage ring (Berlin, Germany) (56) equipped with a PILATUS 6M detector (Company-REF), with a 0.1 ° oscillation and exposure time of 0.3 s per frame. Diffraction images were processed using XDS (41). Crystal parameters and data collection statistics are given in Supplementary Table S3. The Gap-$SO_3H$ structure was solved by molecular replacement with Molrep (71) using the structure of the Gap apoenzyme (PDB entry 3LC7; [57]) as a model. The final model of the Gap-$SO_3H$ was generated by iterative rounds of manual model building using Coot (20)

and automated refinement using the phenix.refine package in PHENIX (1) with the inclusion of TLS parameters generated by the TLSMD server (59). Coordinates and structure factor amplitudes have been deposited in the Protein Data Bank (4) under the accession code 5T73 and will be released upon publication.

### *Molecular docking of BSH into the Gap active site*

To model a covalent complex between BSH and the *S. aureus* Gap active site Cys151, docking experiments were performed with the holo form containing NAD [PDB code: 3LVF chain R, (57)] as well as the apo form [PDB code: 3LC7 chain O, (57)] of the enzyme. Before molecular docking, both protein structures were prepared using the protein preparation wizard (68) in the Schrodinger software (Release 2016–1) graphical user interface Maestro. Hydrogen was added according to the protonation states at pH of 7.0 as predicted by PROPKA, bond orders were assigned, and disulfide bonds were allocated. Water with less than three hydrogen bonds to nonwater residues was removed and minimization of heavy atoms was performed using OPLS3. The BSH structure was obtained from Pubchem (ID: CID 42614123) and processed with the ligand preparation wizard. The ligand was protonated at pH of $7.0 \pm 2.0$ using Epik (28). Covalent molecular docking was performed using CovDock (79), which combines the two programs Glide (23) for docking and Prime (39, 40) for minimization. Cysteine 151 was set as reactive residue, and the reaction type was disulfide formation. All atom positions were fixed, except for the targeted residue and the ligand. Covalent docking was performed with default options and the poses were ranked according to the Prime energy.

## Acknowledgments

This work was supported by a grant from the Deutsche Forschungsgemeinschaft (AN746/4-1) within the SPP1710 on Thiol-based Redox switches, by the DFG grants AN746/3-1 and project C1 of the Research Training Group GRK1947, and by the ERC Consolidator Grant (GA 615585) MYCOTHIOLOME to H.A. Protein crystal structure analysis was supported by an Alexander von Humboldt postdoc fellowship to A.J.P.-B. Molecular docking was supported by the Klaus Tschira Foundation to L.T, K.K., and F.G. The authors would like to thank Sandra Maaß and Dörte Becher (University of Greifswald) for MS of the ICAT-labeled peptides. MS of the over-oxidized Gap was performed at the Centre for Chemical Microscopy (ProVIS) at the Helmholtz Centre for Environmental Research, which is supported by European regional development funds (EFRE-Europe Funds Saxony) and the Helmholtz Association. The authors are grateful to Ambrose Cheung for the kind gift of *S. aureus* USA300 *bshA* mutant.

## Author Disclosure Statement

No competing financial interests exist.

## References

1. Adams PD, Afonine PV, Bunkoczi G, Chen VB, Davis IW, Echols N, Headd JJ, Hung LW, Kapral GJ, Grosse-Kunstleve RW, McCoy AJ, Moriarty NW, Oeffner R, Read RJ, Richardson DC, Richardson JS, Terwilliger TC, and Zwart PH. PHENIX: a comprehensive Python-based system for macromolecular structure solution. *Acta Crystallogr D Biol Crystallogr* 66: 213–221, 2010.
2. Archer GL. *Staphylococcus aureus*: a well-armed pathogen. *Clin Infect Dis* 26: 1179–1181, 1998.
3. Bedhomme M, Adamo M, Marchand CH, Couturier J, Rouhier N, Lemaire SD, Zaffagnini M, and Trost P. Glutathionylation of cytosolic glyceraldehyde-3-phosphate dehydrogenase from the model plant *Arabidopsis thaliana* is reversed by both glutaredoxins and thioredoxins in vitro. *Biochem J* 445: 337–347, 2012.
4. Berman HM, Westbrook J, Feng Z, Gilliland G, Bhat TN, Weissig H, Shindyalov IN, and Bourne PE. The Protein Data Bank. *Nucleic Acids Res* 28: 235–242, 2000.
5. Blanc B, Gerez C, and Ollagnier de Choudens S. Assembly of Fe/S proteins in bacterial systems: biochemistry of the bacterial ISC system. *Biochim Biophys Acta* 1853: 1436–1447, 2015.
6. Bonn F, Bartel J, Büttner K, Hecker M, Otto A, and Becher D. Picking vanished proteins from the void: how to collect and ship/share extremely dilute proteins in a reproducible and highly efficient manner. *Anal Chem* 86: 7421–7427, 2014.
7. Botello-Morte L, Pellicer S, Sein-Echaluce VC, Contreras LM, Neira JL, Abian O, Velazquez-Campoy A, Peleato ML, Fillat MF, and Bes MT. Cysteine mutational studies provide insight into a thiol-based redox switch mechanism of metal and DNA binding in FurA from Anabaena sp. PCC 7120. *Antioxid Redox Signal* 24: 173–185, 2016.
8. Boucher HW and Corey GR. Epidemiology of methicillin-resistant *Staphylococcus aureus*. *Clin Infect Dis* 46 Suppl 5: S344–S349, 2008.
9. Brandes N, Reichmann D, Tienson H, Leichert LI, and Jakob U. Using quantitative redox proteomics to dissect the yeast redoxome. *J Biol Chem* 286: 41893–41903, 2011.
10. Brandes N, Schmitt S, and Jakob U. Thiol-based redox switches in eukaryotic proteins. *Antioxid Redox Signal* 11: 997–1014, 2009.
11. Chen PR, Bae T, Williams WA, Duguid EM, Rice PA, Schneewind O, and He C. An oxidation-sensing mechanism is used by the global regulator MgrA in *Staphylococcus aureus*. *Nat Chem Biol* 2: 591–595, 2006.
12. Chen PR, Brugarolas P, and He C. Redox signaling in human pathogens. *Antioxid Redox Signal* 14: 1107–1118, 2011.
13. Chen PR, Nishida S, Poor CB, Cheng A, Bae T, Kuechenmeister L, Dunman PM, Missiakas D, and He C. A new oxidative sensing and regulation pathway mediated by the MgrA homologue SarZ in *Staphylococcus aureus*. *Mol Microbiol* 71: 198–211, 2009.
14. Chi BK, Busche T, Van Laer K, Bäsell K, Becher D, Clermont L, Seibold GM, Persicke M, Kalinowski J, Messens J, and Antelmann H. Protein S-mycothiolation functions as redox-switch and thiol protection mechanism in *Corynebacterium glutamicum* under hypochlorite stress. *Antioxid Redox Signal* 20: 589–605, 2014.
15. Chi BK, Gronau K, Mäder U, Hessling B, Becher D, and Antelmann H. S-bacillithiolation protects against hypochlorite stress in *Bacillus subtilis* as revealed by transcriptomics and redox proteomics. *Mol Cell Proteomics* 10: M111.009506, 2011.
16. Chi BK, Roberts AA, Huyen TT, Bäsell K, Becher D, Albrecht D, Hamilton CJ, and Antelmann H. S-bacillithiolation protects conserved and essential proteins against hypochlorite stress in firmicutes bacteria. *Antioxid Redox Signal* 18: 1273–1295, 2013.

17. Davies MJ. Myeloperoxidase-derived oxidation: mechanisms of biological damage and its prevention. *J Clin Biochem Nutr* 48: 8–19, 2011.
18. delCardayre SB, Stock KP, Newton GL, Fahey RC, and Davies JE. Coenzyme A disulfide reductase, the primary low molecular weight disulfide reductase from *Staphylococcus aureus*. Purification and characterization of the native enzyme. *J Biol Chem* 273: 5744–5751, 1998.
19. Deng X, Weerapana E, Ulanovskaya O, Sun F, Liang H, Ji Q, Ye Y, Fu Y, Zhou L, Li J, Zhang H, Wang C, Alvarez S, Hicks LM, Lan L, Wu M, Cravatt BF, and He C. Proteome-wide quantification and characterization of oxidation-sensitive cysteines in pathogenic bacteria. *Cell Host Microbe* 13: 358–370, 2013.
20. Emsley P, Lohkamp B, Scott WG, and Cowtan K. Features and development of Coot. *Acta Crystallogr D Biol Crystallogr* 66: 486–501, 2010.
21. Fomenko DE and Gladyshev VN. Comparative genomics of thiol oxidoreductases reveals widespread and essential functions of thiol-based redox control of cellular processes. *Antioxid Redox Signal* 16: 193–201, 2012.
22. Foster TJ. The *Staphylococcus aureus* ''superbug''. *J Clin Invest* 114: 1693–1696, 2004.
23. Friesner RA, Murphy RB, Repasky MP, Frye LL, Greenwood JR, Halgren TA, Sanschagrin PC, and Mainz DT. Extra precision glide: docking and scoring incorporating a model of hydrophobic enclosure for protein-ligand complexes. *J Med Chem* 49: 6177–6196, 2006.
24. Gaballa A, Chi BK, Roberts AA, Becher D, Hamilton CJ, Antelmann H, and Helmann JD. Redox regulation in *Bacillus subtilis*: the bacilliredoxins BrxA(YphP) and BrxB(YqiW) function in de-bacillithiolation of S-bacillithiolated OhrR and MetE. *Antioxid Redox Signal* 21: 357–367, 2014.
25. Gaballa A, Newton GL, Antelmann H, Parsonage D, Upton H, Rawat M, Claiborne A, Fahey RC, and Helmann JD. Biosynthesis and functions of bacillithiol, a major low-molecular-weight thiol in Bacilli. *Proc Natl Acad Sci U S A* 107: 6482–6486, 2010.
26. Graumann J, Lilie H, Tang X, Tucker KA, Hoffmann JH, Vijayalakshmi J, Saper M, Bardwell JC, and Jakob U. Activation of the redox-regulated molecular chaperone Hsp33—a two-step mechanism. *Structure* 9: 377–387, 2001.
27. Gray MJ, Wholey WY, and Jakob U. Bacterial responses to reactive chlorine species. *Annu Rev Microbiol* 67: 141–160, 2013.
28. Greenwood JR, Calkins D, Sullivan AP, and Shelley JC. Towards the comprehensive, rapid, and accurate prediction of the favorable tautomeric states of drug-like molecules in aqueous solution. *J Comput Aided Mol Des* 24: 591–604, 2010.
29. Hampton MB, Kettle AJ, and Winterbourn CC. Involvement of superoxide and myeloperoxidase in oxygen-dependent killing of *Staphylococcus aureus* by neutrophils. *Infect Immun* 64: 3512–3517, 1996.
30. Hawkins CL, Pattison DI, and Davies MJ. Hypochlorite-induced oxidation of amino acids, peptides and proteins. *Amino Acids* 25: 259–274, 2003.
31. Helmann JD. Bacillithiol, a new player in bacterial redox homeostasis. *Antioxid Redox Signal* 15: 123–133, 2011.
32. Helmann JD. Specificity of metal sensing: iron and manganese homeostasis in *Bacillus subtilis*. *J Biol Chem* 289: 28112–28120, 2014.
33. Herrmann JM, Becker K, and Dick TP. Highlight: dynamics of thiol-based redox switches. *Biol Chem* 396: 385–387, 2015.
34. Hildebrandt T, Knuesting J, Berndt C, Morgan B, and Scheibe R. Cytosolic thiol switches regulating basic cellular functions: GAPDH as an information hub? *Biol Chem* 396: 523–537, 2015.
35. Hillion M and Antelmann H. Thiol-based redox switches in prokaryotes. *Biol Chem* 396: 415–444, 2015.
36. Horsburgh MJ, Clements MO, Crossley H, Ingham E, and Foster SJ. PerR controls oxidative stress resistance and iron storage proteins and is required for virulence in *Staphylococcus aureus*. *Infect Immun* 69: 3744–3754, 2001.
37. Ilbert M, Graf PC, and Jakob U. Zinc center as redox switch—new function for an old motif. *Antioxid Redox Signal* 8: 835–846, 2006.
38. Ilbert M, Horst J, Ahrens S, Winter J, Graf PC, Lilie H, and Jakob U. The redox-switch domain of Hsp33 functions as dual stress sensor. *Nat Struct Mol Biol* 14: 556–563, 2007.
39. Jacobson MP, Friesner RA, Xiang Z, and Honig B. On the role of the crystal environment in determining protein side-chain conformations. *J Mol Biol* 320: 597–608, 2002.
40. Jacobson MP, Pincus DL, Rapp CS, Day TJ, Honig B, Shaw DE, and Friesner RA. A hierarchical approach to all-atom protein loop prediction. *Proteins* 55: 351–367, 2004.
41. Kabsch W. Xds. *Acta Crystallogr D Biol Crystallogr* 66: 125–132, 2010.
42. Kay KL, Hamilton CJ, and Le Brun NE. Mass spectrometry of *B. subtilis* CopZ: Cu(i)-binding and interactions with bacillithiol. *Metallomics* 8: 709–719, 2016.
43. Kehr S, Jortzik E, Delahunty C, Yates JR, 3rd, Rahlfs S, and Becker K. Protein S-glutathionylation in malaria parasites. *Antioxid Redox Signal* 15: 2855–2865, 2011.
44. Klebanoff SJ, Kettle AJ, Rosen H, Winterbourn CC, and Nauseef WM. Myeloperoxidase: a front-line defender against phagocytosed microorganisms. *J Leukoc Biol* 93: 185–198, 2013.
45. Kublik A, Deobald D, Hartwig S, Schiffmann CL, Andrades A, von Bergen M, Sawers RG, and Adrian L. Identification of a multi-protein reductive dehalogenase complex in *Dehalococcoides mccartyi* strain CBDB1 suggests a protein-dependent respiratory electron transport chain obviating quinone involvement. *Environ Microbiol* 18: 3044–3056, 2016.
46. Kumsta C and Jakob U. Redox-regulated chaperones. *Biochemistry* 48: 4666–4676, 2009.
47. Lee JW, Soonsanga S, and Helmann JD. A complex thiolate switch regulates the *Bacillus subtilis* organic peroxide sensor OhrR. *Proc Natl Acad Sci U S A* 104: 8743–8748, 2007.
48. Leichert LI, Gehrke F, Gudiseva HV, Blackwell T, Ilbert M, Walker AK, Strahler JR, Andrews PC, and Jakob U. Quantifying changes in the thiol redox proteome upon oxidative stress in vivo. *Proc Natl Acad Sci U S A* 105: 8197–8202, 2008.
49. Lindemann C and Leichert LI. Quantitative redox proteomics: the NOxICAT method. *Methods Mol Biol* 893: 387–403, 2012.
50. Livermore DM. Antibiotic resistance in staphylococci. *Int J Antimicrob Agents* 16 Suppl 1: S3–S10, 2000.
51. Loi VV, Harms M, Müller M, Huyen NT, Hamilton CJ, Hochgräfe F, Pané-Farré J, and Antelmann H. Real-time imaging of the bacillithiol redox potential in the human pathogen *Staphylococcus aureus* using a genetically encoded

bacilliredoxin-fused redox biosensor. *Antioxid Redox Signal* 2016 [Epub ahead of print]; DOI: 10/1089.ars.2016.6733.
52. Loi VV, Rossius M, and Antelmann H. Redox regulation by reversible protein S-thiolation in bacteria. *Front Microbiol* 6: 187, 2015.
53. Lowy FD. *Staphylococcus aureus* infections. *N Engl J Med* 339: 520–532, 1998.
54. Makarova KS, Ponomarev VA, and Koonin EV. Two C or not two C: recurrent disruption of Zn-ribbons, gene duplication, lineage-specific gene loss, and horizontal gene transfer in evolution of bacterial ribosomal proteins. *Genome Biol* 2: 14, 2001.
55. Mallett TC, Wallen JR, Karplus PA, Sakai H, Tsukihara T, and Claiborne A. Structure of coenzyme A-disulfide reductase from *Staphylococcus aureus* at 1.54 A resolution. *Biochemistry* 45: 11278–11289, 2006.
56. Mueller U, Forster R, Hellmig M, Huschmann FU, Kastner A, Malecki P, Puhringer S, Rower M, Sparta K, and Steffien M. The macromolecular crystallography beamlines at BESSY II of the Helmholtz-Zentrum Berlin: current status and perspectives. *Eur Phys J Plus* 130: 141, 2015.
57. Mukherjee S, Dutta D, Saha B, and Das AK. Crystal structure of glyceraldehyde-3-phosphate dehydrogenase 1 from methicillin-resistant *Staphylococcus aureus* MRSA252 provides novel insights into substrate binding and catalytic mechanism. *J Mol Biol* 401: 949–968, 2010.
58. Newton GL, Rawat M, La Clair JJ, Jothivasan VK, Budiarto T, Hamilton CJ, Claiborne A, Helmann JD, and Fahey RC. Bacillithiol is an antioxidant thiol produced in Bacilli. *Nat Chem Biol* 5: 625–627, 2009.
59. Painter J and Merritt EA. LSMD web server for the generation of multi-group TLS models. *J Appl Crystallogr* 39: 109–111, 2006.
60. Pattison DI and Davies MJ. Absolute rate constants for the reaction of hypochlorous acid with protein side chains and peptide bonds. *Chem Res Toxicol* 14: 1453–1464, 2001.
61. Peralta D, Bronowska AK, Morgan B, Doka E, Van Laer K, Nagy P, Grater F, and Dick TP. A proton relay enhances $H_2O_2$ sensitivity of GAPDH to facilitate metabolic adaptation. *Nat Chem Biol* 11: 156–163, 2015.
62. Polgar L. Ion-pair formation as a source of enhanced reactivity of the essential thiol group of D-glyceraldehyde-3-phosphate dehydrogenase. *Eur J Biochem* 51: 63–71, 1975.
63. Poor CB, Chen PR, Duguid E, Rice PA, and He C. Crystal structures of the reduced, sulfenic acid, and mixed disulfide forms of SarZ, a redox active global regulator in *Staphylococcus aureus*. *J Biol Chem* 284: 23517–23524, 2009.
64. Posada AC, Kolar SL, Dusi RG, Francois P, Roberts AA, Hamilton CJ, Liu GY, and Cheung A. Importance of bacillithiol in the oxidative stress response of *Staphylococcus aureus*. *Infect Immun* 82: 316–332, 2014.
65. Pother DC, Gierok P, Harms M, Mostertz J, Hochgrafe F, Antelmann H, Hamilton CJ, Borovok I, Lalk M, Aharonowitz Y, and Hecker M. Distribution and infection-related functions of bacillithiol in *Staphylococcus aureus*. *Int J Med Microbiol* 303: 114–123, 2013.
66. Ralser M, Wamelink MM, Kowald A, Gerisch B, Heeren G, Struys EA, Klipp E, Jakobs C, Breitenbach M, Lehrach H, and Krobitsch S. Dynamic rerouting of the carbohydrate flux is key to counteracting oxidative stress. *J Biol* 6: 10, 2007.
67. Rodriguez-Granillo A and Wittung-Stafshede P. Tuning of copper-loop flexibility in *Bacillus subtilis* CopZ copper chaperone: role of conserved residues. *J Phys Chem B* 113: 1919–1932, 2009.
68. Sastry GM, Adzhigirey M, Day T, Annabhimoju R, and Sherman W. Protein and ligand preparation: parameters, protocols, and influence on virtual screening enrichments. *J Comput Aided Mol Des* 27: 221–234, 2013.
69. Schuppe-Koistinen I, Moldeus P, Bergman T, and Cotgreave IA. S-thiolation of human endothelial cell glyceraldehyde-3-phosphate dehydrogenase after hydrogen peroxide treatment. *Eur J Biochem* 221: 1033–1037, 1994.
70. Sun F, Ding Y, Ji Q, Liang Z, Deng X, Wong CC, Yi C, Zhang L, Xie S, Alvarez S, Hicks LM, Luo C, Jiang H, Lan L, and He C. Protein cysteine phosphorylation of SarA/MgrA family transcriptional regulators mediates bacterial virulence and antibiotic resistance. *Proc Natl Acad Sci U S A* 109: 15461–15466, 2012.
71. Vagin A and Teplyakov A. Molecular replacement with MOLREP. *Acta Crystallogr D Biol Crystallogr* 66: 22–25, 2010.
72. Vospelnikova ND, Safronova MI, Shuvalova ER, Baratova LA, Kniazev SP, and Nagradova NK. Identification of an arginine residue important for catalytic activity in the primary structure of D-glyceraldehyde 3-phosphate dehydrogenase. Studies with the rat skeletal-muscle enzyme. *Biochem J* 199: 757–765, 1981.
73. Weber H, Engelmann S, Becher D, and Hecker M. Oxidative stress triggers thiol oxidation in the glyceraldehyde-3-phosphate dehydrogenase of *Staphylococcus aureus*. *Mol Microbiol* 52: 133–140, 2004.
74. Winterbourn CC and Hampton MB. Thiol chemistry and specificity in redox signaling. *Free Radic Biol Med* 45: 549–561, 2008.
75. Winterbourn CC and Kettle AJ. Redox reactions and microbial killing in the neutrophil phagosome. *Antioxid Redox Signal* 18: 642–660, 2013.
76. Winterbourn CC, Kettle AJ, and Hampton MB. Reactive oxygen species and neutrophil function. *Annu Rev Biochem* 85: 765–792, 2016.
77. Wolf C, Hochgräfe F, Kusch H, Albrecht D, Hecker M, and Engelmann S. Proteomic analysis of antioxidant strategies of *Staphylococcus aureus*: diverse responses to different oxidants. *Proteomics* 8: 3139–3153, 2008.
78. Zaffagnini M, Bedhomme M, Groni H, Marchand CH, Puppo C, Gontero B, Cassier-Chauvat C, Decottignies P, and Lemaire SD. Glutathionylation in the photosynthetic model organism *Chlamydomonas reinhardtii*: a proteomic survey. *Mol Cell Proteomics* 11: M111 014142, 2012.
79. Zhu K, Borrelli KW, Greenwood JR, Day T, Abel R, Farid RS, and Harder E. Docking covalent inhibitors: a parameter free approach to pose prediction and scoring. *J Chem Inf Model* 54: 1932–1940, 2014.

Address correspondence to:
*Prof. Haike Antelmann*
*Institute for Biology-Microbiology*
*Freie Universität Berlin*
*Berlin D-14195*
*Germany*

*E-mail:* haike.antelmann@fu-berlin.de

Date of first submission to ARS Central, September 14, 2016; date of final revised submission, December 6, 2016; date of acceptance, December 7, 2016.

**Abbreviations Used**

1,3-BPG = 1,3-bis-phosphoglycerate
BrxAGC = bacilliredoxin active site mutant
BrxCGA = bacilliredoxin resolving Cys mutant
BSH = bacillithiol
*bshA* = gene for BSH glycosyltransferase
BSSB = oxidized bacillithiol disulfide
Cdr = CoASH disulfide reductase
CoASH = coenzymeA
CV = coefficient of variation
Cys = cysteine
DTT = dithiothreitol
EDTA = ethylenediaminetetraacetic acid
G3P = glyceraldehyde-3-phosphate
Gap = glyceraldehyde-3-phosphate dehydrogenase
Gap-$SO_3H$ = Gap sulfonic acid
Gap-SSB = *S*-bacillithiolated Gap
GlcNAc = N-acetyl glucoseamine
$H_2O_2$ = hydrogen peroxide
HOCl = hypochlorous acid
ICAT = isotope-coded affinity tag
IMP = inosine 5′-monophosphate
IPTG = isopropyl-$\beta$-D-thiogalactopyranoside
LB = Luria bertani
LC = liquid chromatography
LMW = low-molecular-weight
LTQ = linear trap quadrupole
Mal = malate
Met = methionine
MPO = myeloperoxidase
MRSA = methicillin-resistant *Staphylococcus aureus*
Mrx1 = mycoredoxin1
MS = mass spectrometry
MS/MS = tandem mass spectrometry
NADH = nicotinamide adenine dinucleotide
NADPH = nicotinamide adenine dinucleotide phosphate
NaOCl = sodium hypochlorite
NEM = N-ethylmaleimide
OxICAT = thiol redox proteomic methods based on the differential labeling of reduced Cys residues with light ICAT and of reversibly oxidized Cys residues with heavy ICAT after reduction using TCEP
protein-SSB = BSH protein mixed disulfide
RNS = reactive nitrogen species
roGFP2 = redox-sensitive green fluorescent protein
ROS = reactive oxygen species
RSA = relative surface accessibility
SDS-PAGE = sodium dodecyl sulfate–polyacrylamide gel electrophoresis
TCEP = Tris (2-carboxyethyl) phosphine
Trx = thioredoxin
TrxR = thioredoxin reductase